AIAA JOURNAL
Vol. 46, No. 7, July 2008

Large-Eddy Simulations of Turbulent Flows in an Axisymmetric Dump Combustor

Asghar Afshari[†] and Farhad A. Jaberi[‡]
Michigan State University, East Lansing, Michigan 48824-1226
and
Tom I-P. Shih[§]
Iowa State University, Ames, Iowa 50011-2271

DOI: 10.2514/1.25467

A hybrid Eulerian–Lagrangian, mathematical/computational methodology is developed and evaluated for large-eddy simulations of turbulent combustion in complex geometries. The formulation for turbulence is based on the standard subgrid-scale stress models. The formulation for subgrid-scale combustion is based on the filtered mass density function and its equivalent stochastic Lagrangian equations. An algorithm based on high-order compact differencing on generalized multiblock grids is developed for numerical solution of the coupled Eulerian–Lagrangian equations. The results obtained by large-eddy simulations/filtered mass density function show the computational method to be more efficient than existing methods for similar hybrid systems. The consistency, convergence, and accuracy of the filtered mass density function and its Lagrangian–Monte Carlo solver is established for both reacting and nonreacting flows in a dump combustor. The results show that the finite difference and the Monte Carlo numerical methods employed are both accurate and consistent. The results for a reacting premixed dump combustor also agree well with available experimental data. Additionally, the results obtained for other nonreacting turbulent flows are found to be in good agreement with the experimental and high-order numerical data. Filtered mass density function simulations are performed to examine the effects of boundary conditions, subgrid-scale models, as well as physical and geometrical parameters on dump-combustor flows. The results generated for combustors with and without an inlet nozzle are found to be similar as long as appropriate boundary conditions are employed.

Nomenclature

C_d	=	Smagorinsky model coefficient
C_Ω	=	coefficient of the stochastic mixing closure
D_i	=	drift coefficient in the SDE
E	=	diffusion coefficient in the SDE
$\tilde{e}$	=	filtered total energy
F, G, H	=	inviscid fluxes
F_L	=	joint scalars filtered mass density function
F_v, G_v, H_v	=	viscous fluxes
$\mathcal{H}$	=	filter function
H_i^{sgs}	=	subgrid heat flux
$\tilde{i}$	=	filtered internal energy
J	=	Jacobian
J_i^α	=	ith component of the molecular flux vector of scalar α
Pr_t	=	turbulent Prandtl number
$\tilde{p}$	=	filtered pressure
T	=	temperature
$\tilde{T}$	=	filtered temperature
t	=	time
U	=	solution vector
$\tilde{u}, \tilde{v}, \tilde{w}$	=	filtered Cartesian velocity components
u_i^+	=	ith component of the stochastic velocity vector
X_i	=	Lagrangian position of the particles
$\mathbf{x}$	=	position vector
x, y, z	=	coordinate direction in physical domain
x_i	=	ith component of the position vector
α_f	=	filtering parameter
Δ	=	filter size in LES model
λ	=	thermal conductivity
μ	=	molecular dynamic viscosity
μ_e	=	effective viscosity
ν_t	=	subgrid-scale turbulent kinematic viscosity
ξ, η, ζ	=	coordinate directions in transformed domain
$\xi_t, \xi_x, \ldots, \zeta_z$	=	metric coefficients
ρ	=	density
σ	=	number of scalars, $\sigma = N_s + 1$
$\boldsymbol{\phi}$	=	scalar vector
ϕ_α	=	compositional value of scalar α
ϕ_α^+	=	compositional value of stochastic scalar α for Monte Carlo particles
$\boldsymbol{\psi}$	=	composition space vector
Ω_m	=	SGS mixing frequency

Subscripts

i, j, k	=	variable numbers

Conventions

$\tilde{}$	=	Favre filtered value; equivalent to $\langle\,\rangle_L$
$\langle\,\rangle_L$	=	Favre filtered value; equivalent to $\tilde{}$
$\langle\,\rangle_\ell$	=	filtered value
$\langle\vert\rangle_L$	=	conditional Favre filtered value
$\odot$	=	dot product between two vectors

Superscripts

(n)	=	index of the Monte Carlo particles
SGS	=	subgrid scale
$+$	=	properties of the stochastic Monte Carlo particles

[*]Received 26 May 2006; revision received 23 December 2007; accepted for publication 14 January 2008.

[†]Graduate Student, Department of Mechanical Engineering; currently Postdoctoral Research Associate, Computational Science and Engineering, 2234 Digital Computer Laboratory, University of Illinois at Urbana–Champaign, Urbana, IL 61801. Student Member AIAA.

[‡]Associate Professor, Department of Mechanical Engineering. Member AIAA.

[§]Professor and Chair, Department of Aerospace Engineering. Associate Fellow AIAA.

I. Introduction

THE performance of the combustor in an air-breathing propulsion system is dependent on the fluid flow, the heat transfer, the mixing of fuel and air, the chemistry, and many other parameters such as the combustor geometry, the operating pressure, and the preheating temperature. Unfortunately, it is difficult to predict the behavior of a combustion system for various operating parameters, and it is expensive and time consuming to develop new ones solely based on experiments. High-fidelity numerical models, such as the large-eddy simulation (LES), can assist in the development of new combustors by providing valuable, time-dependent spatial data for a wide range of operating conditions.

During the past two decades, LES-based models have been used to predict turbulent reacting flows in various flow configurations with different subgrid-scale (SGS) combustion closures [1–28]. Recently, Jaberi et al. [15] developed a probability density function (PDF) based SGS model termed the filtered mass density function (FMDF) for variable density flows in which the effects of reaction is closed but those of the unresolved turbulent motion and subgrid mixing are modeled. The fundamental property of FMDF is that it explicitly accounts for the SGS scalar fluctuations. The encouraging results generated by FMDF warrant its extension and application to more complicated flows.

Previous PDF modeling research on turbulent reacting flows has pursued two different directions. In one, the focus has been on developing models for complex configurations and practical combustion-device geometry [29,30]. The numerical methods developed for this purpose so far are not appropriate for LES/FMDF due to their limited accuracy and several other issues discussed here and elsewhere [31]. In the other, the focus has been on extending models to study variable density reacting flows with complicated kinetics models [15]. Examples include nonpremixed, premixed, and partially-premixed gaseous turbulent flames [15,32–35]. These studies have often been limited to relatively simple geometries (e.g., axisymmetric and planner jets).

One of the most common geometrical configurations for the combustors in gas turbine and ramjet engines is the dump combustor, which is a sudden-expansion configuration with a stationary recirculation zone for flame stabilization. A number of experimental [36–44] and numerical investigations [45–52] have been carried out on this flow configuration. For example, the experimental work of Stieglmeier et al. [39] for an axisymmetric sudden expansion with different inlet diffusers indicates that the flowfield inside the combustor is strongly influenced by the diffuser geometry. Ahmed and Nejad [40] measured velocity and low-frequency pressure oscillations in the dump combustor of a ramjet engine [40] and found significant differences between reacting and nonreacting cases. They also indicated that the intensity and frequency of the oscillations are dependent on the inlet velocity, combustor length, and equivalence ratio. Lieuwen and Zinn [42] investigated the accuracy of the common experimental method that estimates the unsteady pressure in the flame region of an unstable combustor from pressure measurements along the combustor wall. They also conducted computational studies to quantify the difference between the acoustic pressures at the wall and flame zone. Their results showed that the duct pressure at the flame and wall regions typically differ in magnitude by a factor of 5 and in phase by about 10 deg. Chuang et al. [45] conducted Reynolds-averaged simulation (RAS) for a heated flow in a dump combustor with swirl. They showed that RAS with the standard k–ε model poorly predicts the mean velocity, and it is necessary to use a better (e.g. Reynolds stress) turbulence model. By using RAS, Guo et al. [46] also studied the inflow swirling effects on the flowfield in a sudden-expansion configuration, with the focus on the unsteady flow behavior. They concluded that imparting swirl causes the mean flow to become unstable and oscillatory. With their numerical model, they were able to predict the precessing vortex core phenomenon. Chuang et al. [48] performed RAS calculations of the swirling flow in a dump combustor with a central V-gutter flame holder and six side inlets. Their results indicated that for a fixed swirl strength, the length of the central recirculation zone is decreased when the V-gutter angle is increased. The combustor outlet velocity in the reacting-flow case is found to be higher than that in the cold-flow case because of the heat release effects. Dailey et al. [49] used LES to study the combustion dynamics, flame-vortex interactions, and vortex breakdown mechanisms in a swirling-flow, dump combustor. For a certain choice of system parameters (combustor length and flow-rate), they found that the heat release has an attenuating effect on the combustion through a reduction in the turbulence intensity. Schlüter et al. [50] applied their integrated LES/RAS methodology to simulate swirling dump-combustor flows. They proposed a method based on a virtual body force to impose Reynolds-averaged velocity fields near the outlet on an LES flow domain to take downstream flow effects (computed by a RAS) into account. Huang et al. [51] performed LES of turbulent combustion in a lean-premixed swirl-stabilized combustor. They identified and quantified several physical processes responsible for driving combustion instabilities, including the mutual coupling between acoustic wave motion, vortex shedding, and flame oscillations. They also studied the mechanisms of energy transfer from chemical reactions in the flame zone and acoustic motions in the combustion chamber. Moin and Apte [52] used a second-order, unstructured numerical method to simulate the swirling, particle-laden cold flow in a coaxial sudden-expansion geometry and validated their models by comparison with the experimental data of Sommerfeld and Qiu [43]. Among the available experimental studies on dump combustors, the experimental studies of Gould et al. [36,37] are of particular interest from a computational viewpoint [38]. This is because various turbulence variables in both nonreacting and reacting conditions were measured. Also, inlet boundary conditions are given, even though they are not completely defined.

The main objective of this study is to develop a reliable and affordable LES/FMDF model for the calculation of turbulent combustion in complex geometries. More specifically, a high-order, structured-grid multiblock, compact finite-difference numerical scheme for complex geometries was developed and tested. Several different SGS stress models were considered. For reacting flows, new algorithms were developed for the implementation of the FMDF. Local consistency requirements between Lagrangian–Monte Carlo (MC) and Eulerian finite-difference (FD) components of LES/FMDF were assessed. It is shown that for isothermal and nonisothermal nonreacting flows and for reacting flows, the filtered scalar and temperature fields as obtained by MC and FD are fully consistent. Validation of the models and methods was partly done by comparing the predicted turbulence and flame statistics by LES/FMDF with the experimental data in nonreacting and reacting flows [36,37].

II. Governing Equations

The LES/FMDF methodology involves a combined set of Eulerian and Lagrangian equations that are solved together for velocity and scalar (temperature and mass fractions) fields. These equations are presented later in two separate sections.

A. Velocity Field—Navier–Stokes Equations for Compressible Fluids

The compressible and Favre filtered form of the conservation equations of mass, momentum, and energy in the generalized coordinates can be written as [53–58]

$$\frac{\partial}{\partial t}JU + \frac{\partial \hat{F}}{\partial \xi} + \frac{\partial \hat{G}}{\partial \eta} + \frac{\partial \hat{H}}{\partial \zeta} = J\hat{S} \tag{1}$$

The spatial filtering operation [59] is given by

$$f(\tilde{\mathbf{x}}, t) = \langle f(\mathbf{x}, t)\rangle_\ell = \int_{-\infty}^{+\infty} f(\mathbf{x}', t)\mathcal{H}(\mathbf{x}', \mathbf{x})\mathrm{d}\mathbf{x}' \tag{2}$$

where $\mathcal{H}$ denotes the filter function, $\langle f(\mathbf{x}, t)\rangle_\ell$ represents the filtered value of the transport variable $f(\mathbf{x}, t)$. In variable density flows it is more convenient to consider the Favre filtered quantity, $\langle f(\mathbf{x}, t)\rangle_L = \langle \rho f\rangle_\ell / \langle \rho\rangle_\ell$. In the preceding equations, t is the time, ξ, η, ζ are coordinate directions in transformed domain, and $J = \partial(x, y, z, t)/\partial(\xi, \eta, \zeta, \tau)$ is the determinant of the transformation

Jacobian. The solution vector JU is given by

$$JU = J\{\bar{\rho}, \bar{\rho}\tilde{u}, \bar{\rho}\tilde{v}, \bar{\rho}\tilde{w}, \bar{\rho}\tilde{E}\} \tag{3}$$

and $\hat{F}$, $\hat{G}$, and $\hat{H}$ fluxes as

$$\hat{F} = J[\xi_t U + \xi_x(F - F_v) + \xi_y(G - G_v) + \xi_z(H - H_v)] \tag{4}$$

$$\hat{G} = J[\eta_t U + \eta_x(F - F_v) + \eta_y(G - G_v) + \eta_z(H - H_v)] \tag{5}$$

$$\hat{H} = J[\zeta_t U + \zeta_x(F - F_v) + \zeta_y(G - G_v) + \zeta_z(H - H_v)] \tag{6}$$

Here $\xi_t, \xi_x, \ldots, \zeta_z$ are the metric coefficients. F, G, and H denote the inviscid fluxes, and, F_v, G_v, and H_v are the viscous fluxes. These are related to filtered variables as follows:

$$F = \{\bar{\rho}\tilde{u}, \bar{\rho}\tilde{u}\tilde{u} + \bar{p}, \bar{\rho}\tilde{v}\tilde{u}, \bar{\rho}\tilde{w}\tilde{u}, (\bar{\rho}\tilde{E} + \bar{p})\tilde{u}\} \tag{7}$$

$$G = \{\bar{\rho}\tilde{v}, \bar{\rho}\tilde{u}\tilde{v}, \bar{\rho}\tilde{v}\tilde{v} + \bar{p}, \bar{\rho}\tilde{v}\tilde{w}, (\bar{\rho}\tilde{E} + \bar{p})\tilde{v}\} \tag{8}$$

$$H = \{\bar{\rho}\tilde{w}, \bar{\rho}\tilde{w}\tilde{u}, \bar{\rho}\tilde{w}\tilde{v}, \bar{\rho}\tilde{w}\tilde{w} + \bar{p}, (\bar{\rho}\tilde{E} + \bar{p})\tilde{w}\} \tag{9}$$

With the operators

$$L_1 = \left[\xi_x\frac{\partial}{\partial\xi} + \eta_x\frac{\partial}{\partial\eta} + \zeta_x\frac{\partial}{\partial\zeta}\right] \tag{10}$$

$$L_2 = \left[\xi_y\frac{\partial}{\partial\xi} + \eta_y\frac{\partial}{\partial\eta} + \zeta_y\frac{\partial}{\partial\zeta}\right] \tag{11}$$

$$L_3 = \left[\xi_z\frac{\partial}{\partial\xi} + \eta_z\frac{\partial}{\partial\eta} + \zeta_z\frac{\partial}{\partial\zeta}\right] \tag{12}$$

one can write the viscous fluxes as

$$F_v = \begin{bmatrix} 0 \\ \mu_e\{2L_1[\tilde{u}] - \frac{2}{3}(L_1[\tilde{u}] + L_2[\tilde{v}] + L_3[\tilde{w}])\} \\ \mu_e(L_1[\tilde{v}] + L_2[\tilde{u}]) \\ \mu_e(L_1[\tilde{w}] + L_3[\tilde{u}]) \\ \tilde{u}F_{v2} + \tilde{v}F_{v3} + \tilde{w}F_{v4} + \lambda L_1[\tilde{T}] + \frac{\bar{\rho}\nu_t}{Pr_t}L_1[\tilde{H}] \end{bmatrix} \tag{13}$$

$$G_v = \begin{bmatrix} 0 \\ \mu_e(L_1[\tilde{v}] + L_2[\tilde{u}]) \\ \mu_e\{2L_2[\tilde{v}] - \frac{2}{3}(L_1[\tilde{u}] + L_2[\tilde{v}] + L_3[\tilde{w}])\} \\ \mu_e(L_2[\tilde{w}] + L_3[\tilde{v}]) \\ \tilde{u}G_{v2} + \tilde{v}G_{v3} + \tilde{w}G_{v4} + \lambda L_2[\tilde{T}] + \frac{\bar{\rho}\nu_t}{Pr_t}L_2[\tilde{H}] \end{bmatrix} \tag{14}$$

$$H_v = \begin{bmatrix} 0 \\ \mu_e(L_1[\tilde{w}] + L_3[\tilde{u}]) \\ \mu_e(L_2[\tilde{w}] + L_3[\tilde{v}]) \\ \mu_e\{2L_3[\tilde{w}] - \frac{2}{3}(L_1[\tilde{u}] + L_2[\tilde{v}] + L_3[\tilde{w}])\} \\ \tilde{u}H_{v2} + \tilde{v}H_{v3} + \tilde{w}H_{v4} + \lambda L_3[\tilde{T}] + \frac{\bar{\rho}\nu_t}{Pr_t}L_3([\tilde{H}]) \end{bmatrix} \tag{15}$$

In the preceding equations, $\tilde{u}$, $\tilde{v}$, and $\tilde{w}$ are the Favre filtered velocity components, $\tilde{T}$ denotes the Favre filtered temperature and λ, ν_t, Pr_t are the thermal conductivity, SGS viscosity and SGS turbulent Prandtl number, respectively. The filtered density and pressure are represented by $\bar{\rho}$ and $\bar{p}$, respectively. Variables F_{vn}, G_{vn}, and H_{vn} are nth components of F_v, G_v, and H_v vectors. Also, in our nonreacting simulations, the source term is a null vector, whereas for reacting simulations it will be computed from the FMDF data. $\tilde{e}$ is the total energy, given by

$$\tilde{e} = \bar{\rho}\tilde{E} = \bar{\rho}\left\{\tilde{i} + \frac{\tilde{u}^2 + \tilde{v}^2 + \tilde{w}^2}{2}\right\} \tag{16}$$

in which $\tilde{i}$ is the Favre filtered internal energy. The SGS energy term is ignored as it is negligible in low-Mach number flows. The effective SGS viscosity (μ_e) is defined as

$$\mu_e = \mu + \bar{\rho}\nu_t \tag{17}$$

where μ is the molecular viscosity. The SGS turbulent kinematic viscosity (ν_t) is computed by one of four models: the Smagorinsky model [60,61], the modified kinetic energy viscosity (MKEV) model [11], the dynamic Smagorinsky model [62–64], and the algebraic renormalization group (RNG) SGS closure [65].

The closure of the subgrid heat flux, H_{ij}^{SGS}, is also based on a gradient-diffusion model [66,67] given by

$$H_i^{\mathrm{SGS}} = -\bar{\rho}\frac{\nu_t}{Pr_t}\frac{\partial\tilde{H}}{\partial x_i}, \qquad \tilde{H} = \tilde{E} + \frac{\bar{p}}{\bar{\rho}} \tag{18}$$

These subgrid terms have been expressed in generalized coordinates [Eqs. (13–15)]. Here, the unresolved viscous work is neglected. Also, in the filtering procedure, mesh nonuniformity is neglected [i.e., filtered value of (metric coefficient times any scalar) is equal to (metric coefficient) times the filtered value of the scalar]. The effects of the SGS stress model on the filtered variables will be discussed later in this paper.

B. Scalar Field—FMDF Equation for Reacting Flows

With $\boldsymbol{\phi}(\mathbf{x}, t) \equiv [\phi_1, \phi_2, \ldots, \phi_\sigma]$ as the scalar array, we can define the FMDF, denoted by F_L, as

$$F_L(\boldsymbol{\psi}; \mathbf{x}, t) \equiv \int_{-\infty}^{+\infty} \rho(\mathbf{x}', t)\zeta[\boldsymbol{\psi}, \boldsymbol{\phi}(\mathbf{x}', t)]\mathcal{H}(\mathbf{x}' - \mathbf{x})\,\mathrm{d}\mathbf{x}' \tag{19}$$

$$\zeta[\boldsymbol{\psi}, \boldsymbol{\phi}(\mathbf{x}, t)] = \delta[\boldsymbol{\psi} - \boldsymbol{\phi}(\mathbf{x}, t)] \equiv \prod_{\alpha=1}^{\sigma}\delta[\psi_\alpha - \phi_\alpha(\mathbf{x}, t)] \tag{20}$$

where δ denotes the delta function and $\boldsymbol{\psi}$ denotes the composition domain of the scalar array. The term $\zeta[\boldsymbol{\phi}, \boldsymbol{\psi}(\mathbf{x}, t)]$ is the fine-grained density [68,69], and Eq. (19) implies that the FMDF is the *mass weighted spatially filtered* value of the fine-grained density.

By applying the method developed by Lundgren [70], Pope [71], and O'Brien [68] to the $\boldsymbol{\phi}$ equation, a transport equation is obtained for the fine-grained density [11]. The transport equation for $F_L(\boldsymbol{\psi}; \mathbf{x}, t)$ is obtained by multiplying the equation for the fine-grained density by the filter function $\mathcal{H}(\mathbf{x}' - \mathbf{x})$ and integrating over $\mathbf{x}'$ space. The final result after some algebraic manipulation is

$$\frac{\partial F_L(\boldsymbol{\psi}; \mathbf{x}, t)}{\partial t} + \frac{\partial[\langle u_i(\mathbf{x}, t)|\boldsymbol{\psi}\rangle_\ell F_L(\boldsymbol{\psi}; \mathbf{x}, t)]}{\partial x_i} = \frac{\partial}{\partial\psi_\alpha}\left[\left\langle\frac{1}{\hat{\rho}(\boldsymbol{\phi})}\frac{\partial J_i^\alpha}{\partial x_i}\middle|\boldsymbol{\psi}\right\rangle_\ell F_L(\boldsymbol{\psi}; \mathbf{x}, t)\right] - \frac{\partial[\hat{S}_\alpha(\boldsymbol{\psi})F_L(\boldsymbol{\psi}; \mathbf{x}, t)]}{\partial\psi_\alpha} \tag{21}$$

where the $\hat{}$ symbol on S_α implies that this variable is only a function of scalars. This is an exact transport equation for the FMDF which can be solved by standard (Eulerian) methods. However, standard numerical methods are very expensive due to added dimensions. In practice, only Lagrangian methods can be used. The last term on the right-hand side of this equation is a closed-form chemical reaction term. The unclosed nature of SGS convection and mixing is indicated by the conditional, filtered values. These terms are modeled in a manner consistent with Reynolds averaging and conventional LES in nonreacting flows. The convection term is decomposed as follows:

$$\langle u_i|\boldsymbol{\psi}\rangle_\ell F_L = \langle u_i\rangle_L F_L + [\langle u_i|\boldsymbol{\psi}\rangle_\ell - \langle u_i\rangle_L]F_L \tag{22}$$

where the second term on the right-hand side denotes the influence of SGS convective flux. This term is modeled as

$$[\langle u_i|\boldsymbol{\psi}\rangle_\ell - \langle u_i\rangle_L]F_L = -\gamma_t \frac{\partial(F_L/\langle\rho\rangle_\ell)}{\partial x_i} \tag{23}$$

The advantage of the decomposition [Eq. (22)] and the subsequent model [Eq. (23)] is that they yield results similar to that in conventional LES [72,73]. The closure adopted for the SGS mixing is based on the linear mean square estimation (LMSE) model [68,74], also known as the IEM (interaction by exchange with the mean) [75],

$$\frac{\partial}{\partial\psi_\alpha}\left[\left\langle -\frac{1}{\hat\rho}\frac{\partial}{\partial x_i}\left(\gamma\frac{\partial\phi_\alpha}{\partial x_i}\right)\middle|\boldsymbol{\psi}\right\rangle_\ell F_L\right] = \frac{\partial}{\partial x_i}\left(\gamma\frac{\partial(F_L/\hat\rho)}{\partial x_i}\right) + \frac{\partial}{\partial\psi_\alpha}[\Omega_m(\psi_\alpha - \langle\phi_\alpha\rangle_L)F_L] \tag{24}$$

where $\Omega_m(\mathbf{x}, t)$ is the frequency of mixing within the subgrid, which is not known a priori. This frequency is modeled as $\Omega_m = C_\Omega(\gamma + \gamma_t)/(\langle\rho\rangle_\ell \Delta_G^2)$ here, but other models can be used. With these models and few minor approximations, the modeled FMDF transport equation becomes

$$\frac{\partial F_L}{\partial t} + \frac{\partial[\langle u_i\rangle_L F_L]}{\partial x_i} = \frac{\partial}{\partial x_i}\left[(\gamma+\gamma_t)\frac{\partial(F_L/\langle\rho\rangle_\ell)}{\partial x_i}\right] + \frac{\partial}{\partial\psi_\alpha}[\Omega_m(\psi_\alpha - \langle\phi_\alpha\rangle_L)F_L] - \frac{\partial[\hat S_\alpha F_L]}{\partial\psi_\alpha} \tag{25}$$

This equation may be integrated to obtain transport equations for the SGS moments. The equation for the first subgrid Favre moment, $\langle\phi_\alpha\rangle_L$ is

$$\frac{\partial(\langle\rho\rangle_\ell\langle\phi_\alpha\rangle_L)}{\partial t} + \frac{\partial(\langle\rho\rangle_\ell\langle u_i\rangle_L\langle\phi_\alpha\rangle_L)}{\partial x_i} = \frac{\partial}{\partial x_i}\left[(\gamma+\gamma_t)\frac{\partial\langle\phi_\alpha\rangle_L}{\partial x_i}\right] + \langle\rho\rangle_\ell\langle S_\alpha\rangle_L \tag{26}$$

where the subscripts in parenthesis are excluded from the summation convention. This equation is identical to the one derived by filtering the scalar equation directly, and employing consistent closures for the subgrid flux and the dissipation. In direct moment closure formulation, however, the terms involving $\langle S_\alpha\rangle_L$ remain unclosed. This indicates that for nonreacting flows the FMDF method is consistent with standard LES methods at the first moment level (and possibly second, if the second moment equation is solved by standard methods).

Ideally, it is not necessary to solve the standard (Eulerian) equations for the energy and scalars in the LES/FMDF methodology because they can be obtained from the FMDF. However, to avoid some of the numerical problems associated with the interactions of Eulerian and Lagrangian fields, the Eulerian energy equation is also solved here with the chemical source term obtained from the FMDF. This is because of the fact that the derivative of pressure becomes very noisy when the MC values of the filtered temperature are used in the equation of state. A conserved scalar equation is also solved by the Eulerian (finite-difference) method only for demonstrating the consistency between the Lagrangian and Eulerian solvers.

The first four components of the source term vector $\hat S$ in Eq. (1) are zero and the fifth component, which is the reaction source term in energy equation, is obtained from a one-step global Arrhenious chemistry model [76] for propane-air combustion. Again, the source term is computed from the FMDF data and is closed.

III. Numerical Solution Procedure

The LES/FMDF methodology is based on two different but coupled mathematical models, namely, 1) the conventional LES equations for the velocity field and 2) the FMDF equation for the scalar (species and temperature) field. The numerical methods used for 1) and 2) are different and hence described later in two separate sections.

A. Eulerian Finite-Difference Method for Velocity Field

In this section, the temporal and spatial discretization of the Eulerian Navier–Stokes equations along with the boundary conditions are described. For any scalar variable, such as a flux component, a metric, or a flow variable, the spatial derivative of the variable in the transformed domain is calculated with a high-order, FD formula. The derivatives of inviscid and viscous fluxes are obtained by first forming the fluxes at the nodes and subsequently using the fourth-order, compact-differencing formula [77,78]. At boundary points, higher-order one-sided formulas are used which retain the tridiagonal form of the interior scheme. All of the time derivatives in the governing equations are approximated by a low-storage three-stage Runge–Kutta (RK) scheme, which belongs to the strong, stability-preserving (SSP), RK family [79,80]. The noise generated by the growth of numerical error at very high-wave number/frequency modes is removed here by using a filtering procedure. This filtering operation is different from the standard LES filtering operation and has no significant effect on the flow variables. Compact differencing, like other central difference schemes, is a nondissipative scheme. In LES and direct numerical simulation (DNS), the application of nondissipative spatial schemes leads to a pileup of energy at the smallest scales of the flow. In this work, a low-pass, high-order, spatial implicit filtering operator [54,81] is used for both interior and near-boundary values. The numerical filtering operation suppresses numerical instabilities arising from mesh nonuniformities and boundary conditions. Filtering is performed at the end of each time step and is applied in each direction. For multiblock cases the data are exchanged between blocks after filtering. We have tested both the fourth- and eighth-order filtering for interior and boundary points, and we have found the effects of filtering on the flow variables to be negligible.

In the multiblock strategy considered here, a series of structured grids of varying sizes and shapes are constructed in such a way that the entire computational domain is covered. By the segmentation of the domain into smaller blocks, the topological problems usually encountered in constructing grids for complex configurations are avoided. The main idea is to construct a halo of cells that surrounds each block and contains information from cells in the neighboring blocks [82]. This halo of cells, when updated at the appropriate times during the numerical solution procedure, allows the flow calculations inside each block to proceed independently of the others. This approach requires the identification of halo cells adjacent to block boundaries and the construction of a list of halo cells and their internal counterparts in other portions of the global mesh. This double halo procedure is needed for evaluation of the flux vectors for the internal cells of each block without using additional cells located outside the block. For a second-order, explicit method, the communication between blocks occurs at every stage of the Runge–Kutta scheme in a way that treats the multiblock grid as if there were only one block with no internal boundaries and no time-lag between blocks. For an implicit method, the accuracy will increase with more overlaps. In the flow solver developed here, data are exchanged between adjacent blocks/domains at the end of each stage of the Runge–Kutta scheme, as well as after each application of the high-wave number, filtering operation.

In this work several types of boundary conditions are considered. All boundary conditions satisfy the mathematical/numerical criteria. For isotropic turbulence, periodic boundary conditions are used in every direction. The inlet boundary conditions have been extensively examined for the dump-combustor simulations. For the case that the computational domain is truncated right at the sudden-expansion point, the results suggest that by floating the temperature (e.g., using $\partial T/\partial x = 0$), fixing density, and computing the pressure through the equation of state, the numerical stability is preserved. For the case with an added nozzle, all tested inlet boundary conditions yield the same results. Also for the inlet boundary condition, the experimental data were used to generate turbulent velocity perturbations based on a multifrequency, random-phase harmonic function. Characteristic

boundary condition [83] coupled with the convective boundary condition is used for the outflow boundary in all of our dump-combustor simulations. No-slip boundary condition is used for the walls.

B. Lagrangian–Monte Carlo Method for Scalar Field

In this study, the scalar (species mass fractions and enthalpy) field, $\boldsymbol{\phi} \equiv \phi_\alpha,\ \alpha = 1, 2, \ldots, N_s + 1$ is obtained from the joint scalar FMDF [15]. The FMDF transport equation is solved by using a Lagrangian–Monte Carlo procedure [69,84]. In this procedure, Eq. (25) is solved indirectly via equivalent stochastic (diffusion) equations. Here, the spatial transport of the FMDF is represented by the general, diffusion process governed by the following stochastic differential equation (SDE) [85,86]:

$$\mathrm{d}X_i(t) = D_i(\mathbf{X}(t), t)\,\mathrm{d}t + E(\mathbf{X}(t), t)\,\mathrm{d}W_i(t) \tag{27}$$

where X_i is the Lagrangian position of a stochastic particle, D_i and E are the drift and diffusion coefficients, respectively, and W_i denotes the Wiener process [87]. The drift and diffusion coefficients are obtained by comparing the Fokker–Plank equation corresponding to Eq. (27) with the FMDF transport [Eq. (25)]

$$E \equiv \sqrt{2(\gamma + \gamma_t)/\langle\rho\rangle_\ell}, \qquad D_i \equiv \langle u_i\rangle_L + \frac{1}{\langle\rho\rangle_\ell}\frac{\partial(\gamma + \gamma_t)}{\partial x_i} \tag{28}$$

The subgrid mixing and reaction terms are implemented by altering the compositional makeup of the particles according to the following SDE:

$$\frac{\mathrm{d}\phi_\alpha^+}{\mathrm{d}t} = -\Omega_m(\phi_\alpha^+ - \langle\phi_\alpha\rangle_L) + \hat{S}_\alpha(\boldsymbol{\phi}^+) \tag{29}$$

where $\phi_\alpha^+ = \phi_\alpha(\mathbf{X}(t), t)$ denotes the scalar value of the particle with the Lagrangian position vector X_i. The solutions of Eqs. (27) and (29) yield the same statistics as those obtained directly from the solution of FMDF transport equation according to the principle of *equivalent systems* [69,88].

Lagrangian methods have been used for simulation of a wide variety of stochastic problems [89,90]. They have been the primary means of solving the PDF in RAS [69,84,91–93] and thus far the primary method of choice for solving FMDF in LES. Typically, the method is implemented by representing the FMDF by an ensemble of N_p particles. These particles carry information pertaining to their positions, $\mathbf{x}^{(n)}(t)$, and scalar values, $\boldsymbol{\phi}^{(n)}(t)$, $n = 1, \ldots, N_p$. This information is updated by the time integration of modeled SDEs (22) based on the Euler–Maruyamma approximation [94]. This approximation advances the position of the nth particle $x^n(t)$ from time level t_k to t_{k+1} according to

$$x_i^n(t_{k+1}) = x_i^n(t_k) + D_i^n(t_k)\Delta t + B^n(t_k)(\Delta t)^{1/2}\zeta_i^n(t_k), \qquad i = 1, 2, 3 \tag{30}$$

where $\zeta_i^n(t_k)$ are independent standardized Gaussian random variables. This formulation preserves the Markovian character of the diffusion processes [95,96] and facilitates affordable computations. Higher-order numerical schemes are available [94], but one must be cautious in using them for LES [11]. Because the diffusion term in the SDEs depends on the stochastic processes, the numerical scheme must be consistent with Ito [97] and Gikhman [98] calculus. Equation (30) exhibits this property.

Although it is possible to simulate the FMDF exclusively via MC methods, the most practical procedure is a hybrid FD/MC method. For flows in complex geometries, there are several important issues in the implementation of hybrid methods that need to be addressed. These issues are partly investigated in the context of RAS/PDF [99,100] and constitute a major element of the computational procedure in the LES/FMDF that is considered in this paper. The attributes of the conventional LES and the FMDF are shown in Fig. 1. The flowchart also shows the redundant variables and the necessary consistency between the FD and MC parts of the hybrid LES/FMDF flow solver. With a hybrid method as such, some of the quantities are obtained by MC, some by FD, and some by *both*. That is, there is a redundancy in the determination of some of the quantities. In general, all of the equations for the filtered quantities can be solved by FD, in which all of the unclosed terms are evaluated by MC. This process can be done at any filtered moment level [101].

An effective method has been developed to search and locate the MC particles in the structured, multiblock Eulerian grid system, which makes the FMDF affordable and feasible for LES of flows in complex geometries. The search and locate operation for MC particles is usually an expensive operation, especially when the grid is unstructured. However, as explained later, for the structured-grid system and special geometry considered in this study we have developed a very efficient and relatively inexpensive algorithm. This algorithm can be used for any complex geometry by considering an appropriate formulation with respect to the nonuniform but still structured grids.

Figure 2a shows the grid lines, MC particles, and imaginary control volumes formed around the grid points in the LES/FMDF. For simplicity, two-dimensional views are shown, even though the procedure is three-dimensional. The thinner lines represent the grid lines of the finite-difference mesh. The thicker lines represent the cell faces of the control volume centered about the intersection of the grid lines. The dots represent the Monte Carlo particles. The control volumes around the grid points are formed by connecting the midpoints of the grid-line segments. In Fig. 2a, the hexagon $a\,b\,c\,d\,e\,f$ is formed around the point O, which is the FD grid point. The particles located inside hexagon $a\,b\,c\,d\,e\,f$ are considered in the ensemble averaging, and point O is a good representative for the center of the hexagon cell. For interpolation, FD grid points are used. As shown in Fig. 2a, when particle p is located inside the quadrilateral $q\,r\,s\,t$ the values at the corners will be used. To perform the ensemble averaging and interpolation for any particle, the hexagon $a\,b\,c\,d\,e\,f$ and the quadrilateral $q\,r\,s\,t$, should be determined. As the procedure is the same to determine the hexagon $a\,b\,c\,d\,e\,f$ and the quadrilateral $q\,r\,s\,t$, here we only describe the method to determine the quadrilateral $q\,r\,s\,t$.

To locate the particle, the first step is to determine the block in which the particle belongs to. When the corresponding block for the particle p is known and the three coordinate indexes of point q are determined, the quadrilateral $q\,r\,s\,t$ is specified. In other words, we only need to determine the i, j, and k (integer coordinate indexes) of point q to know the particle location with respect to the Eulerian grid system. To determine the i component of q, the auxiliary vectors **sp**, **sq**, and **A** are defined. **A** is the normal vector to **st** and could easily be formed (the direction of **A** could be either way). With this, $G(q)$ is defined as follows ($\odot \equiv$ dot product between two vectors):

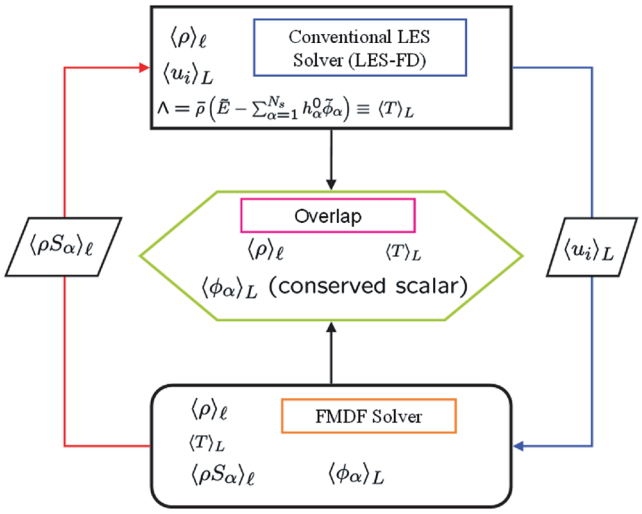

Fig. 1 The attributes of LES/FMDF methodology and its LES/FD and FMDF/MC subcomponents.

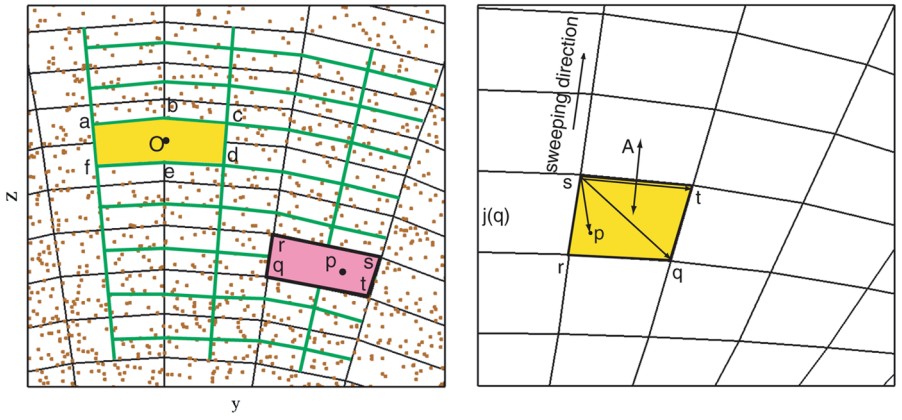

a) b)

Fig. 2 Schematic description of a) grid points, Monte Carlo particles, and control volumes around the grid points, b) the process for determining the j component of point q.

$$G(q) = (\mathbf{sp} \odot \mathbf{A})(\mathbf{sq} \odot \mathbf{A}) \tag{31}$$

If $G(q)$ is positive, the particle p and point q lie on the same side of $\mathbf{st}$, meaning p is located at the east side of $\mathbf{st}$. We can assume the sweeping start point to be $i = 1$ and that sweeping is performed in the direction of increasing i. The first grid point with $G > 0$ is q. A similar procedure is used in other directions as shown in Fig. 2b. As the i component of q is determined, the k component could be specified by searching in a grid-plane. By knowing the i and k components, j is determined only by sweeping in a segment formed by the grid lines. To reduce the cost of the searching procedure, the starting points for sweeping are determined by previous values (which are stored for each particle) and the moving direction of the particle, which is based on the velocity of the particle. The preceding numerical scheme is applicable to any curvilinear grid.

To interpolate the properties needed in particle locations, a (coupled) linear interpolation is applied in three grid-line directions. Statistical information, for example, filtered values, at any point are obtained by considering an ensemble of N_E computational particles residing within an ensemble domain of side length Δ_E centered around the grid points. Here, ensemble averaging of particles is employed in a way that there is an acceptable number of particles in ensemble domain. As particles move in physical space, the ensemble averaging domain is chosen so that $N_{p,\min} \leq N_p \leq N_{p,\max}$. This means that if the number of particles is lower than the minimum number specified, a bigger ensemble domain is considered, or if it exceeds a maximum value, a smaller ensemble domain is considered. This approach is an alternative for cloning and annihilation in which property distributions are not exactly preserved. Different values of $N_{p,\min}$ were examined and it was insured that $N_{p,\min}$ was sufficiently high.

IV. Results

To validate the mathematical/computational model for the velocity field, DNS and LES of various nonreacting turbulent flows were conducted. The results obtained from these simulations were found to be in good agreement with the available experimental data and solutions obtained by validated, high-order numerical methods. Sample results are shown here.

In Fig. 3, the predicted turbulent energy spectrum by DNS with our high-order FD method for an isotropic turbulent flow are compared with those obtained by the spectral and finite volume (FV) methods. In these simulations, the initial Reynolds number based on the turbulence intensity and the Taylor microscale is 35, and a 64^3 mesh is used. Figure 3 shows a comparison after about four eddy turnover times (the eddy turnover time is $\sim$3.5). The FD results are filtered with an implicit fourth- and eighth-order filter function (α_f is the filtering parameter [53,54]). As mentioned before, these high-order filtering operations are employed for removing the numerical noise at the smallest turbulent scales and do not have significant effects on the turbulent statistics. The comparison between the high-order FD and spectral results in Fig. 3 indicate the accuracy of the fourth-order FD method with fourth-order implicit filtering, even though the FD predictions are slightly improved when an eighth-order filtering is employed. However, the second-order FV method seems to be too dissipative and cannot correctly predict the energy spectrum. The results at other times indicate similar trends and are not shown here. In the FV method, instead of low-pass filtering, a second-order, upwind, numerical dissipation was added to the equations to preserve the numerical stability. With a refined grid, the second-order FV and the fourth-order FD generate the same results. Close examination of the results for different cases indicates that the inaccuracies in the second-order FV is not just due to grid resolution but higher numerical diffusion from upwinding. For the second-order FV method, the grid must be much finer to reduce the numerical error to an acceptable level so that the physics can be accurately resolved. The purpose of the comparison made between second-order and fourth-order schemes is not to show the superiority of the latter. This is expected. The purpose is to show the importance of using high-order numerical schemes in LES.

As examples of inhomogeneous flows, turbulent, round, and planar jets have been also considered for the validation of our flow solver. Analysis of DNS and LES data for these flows indicates that the physical features of the flow are correctly captured by our high-order FD numerical scheme. The LES predictions for a turbulent round jet are also found to be in good agreement [31] with the experimental data [102]. The jet results are not presented in this paper.

As mentioned before, the focus of this paper is on the large-eddy simulations of turbulent flows in an axisymmetric dump combustor. Gould et al. [36,37] have conducted laboratory experiments on this configuration for nonreacting and reacting flows. Figure 4 illustrates the experimental setup and the grid system for the dump combustor considered in this study. The three-block grid system shown in Fig. 4d is sufficient for simulations of flow in the dump combustor

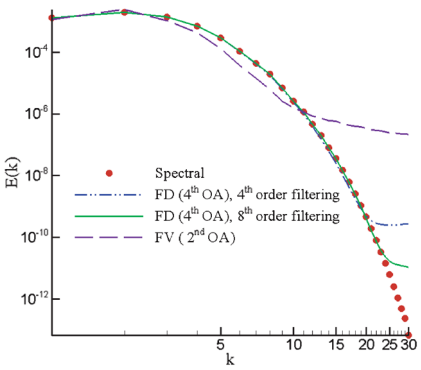

Fig. 3 A comparison of energy spectrum obtained with different numerical schemes at time = 15.

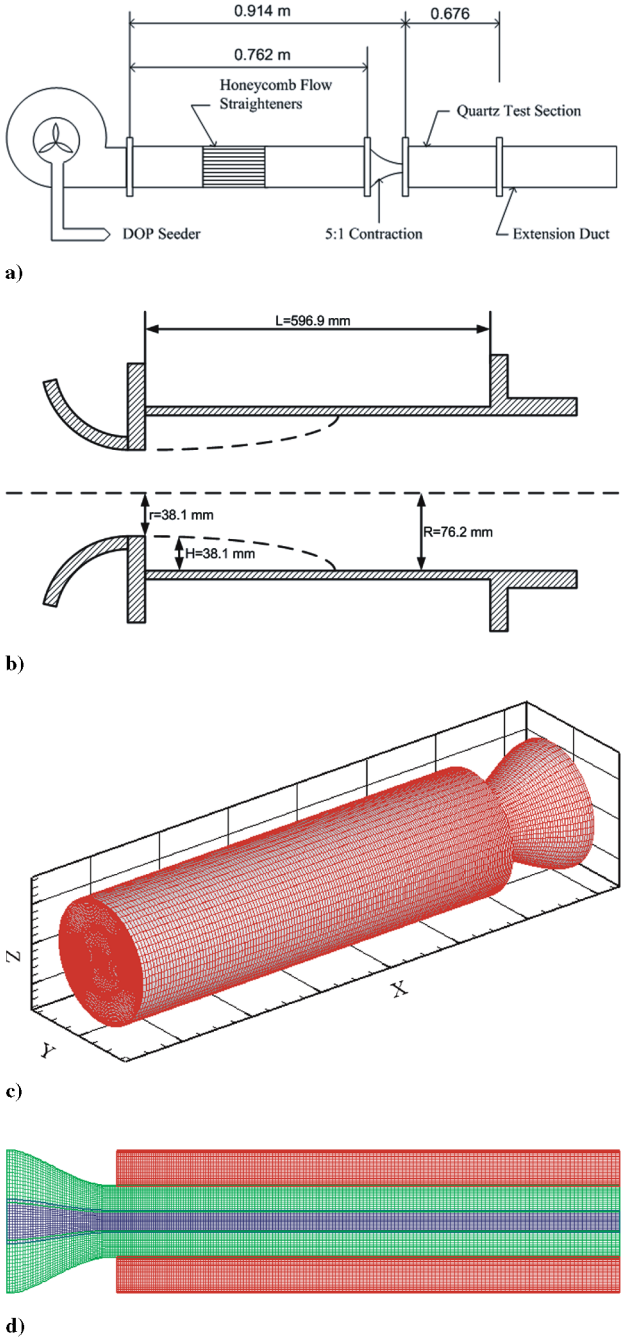

Fig. 4 Schematic perspective of the a) experimental setup, b) dump-combustor test section, c) 3-D grid layout, and d) 2-D grid layout.

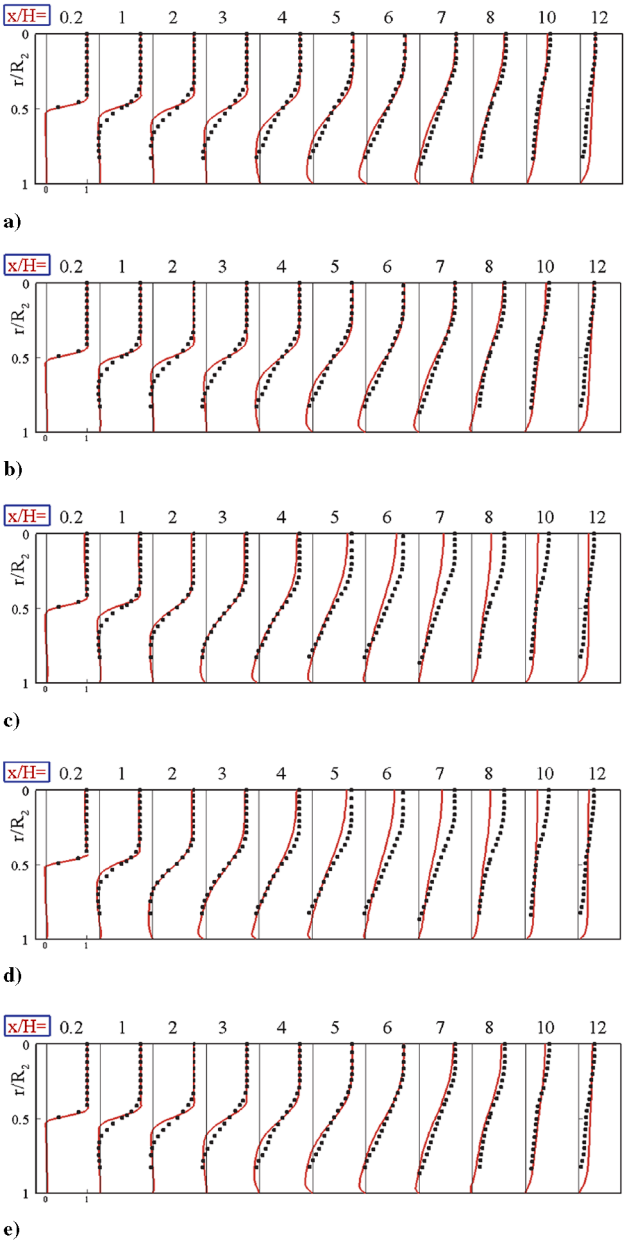

Fig. 5 Comparison between experiment and LES with different SGS models for mean axial velocity (●, experiment; solid lines, LES.) a) Smagorinsky model ($C_d = 0.01$), b) Smagorinsky model ($C_d = 0.028$), c) MKEV model, d) dynamic Smagorinsky model, and e) RNG model. The LES calculations are for the case without the inlet nozzle.

even though the grid resolution is varied. The numerical scheme developed here is not limited to this relatively simple grid system and can be applied to much more complicated geometries with any number of blocks. The dump-combustor results as obtained by LES/FMDF are discussed in three different sections. First, we consider the nonreacting LES results at relatively high-Reynolds number (115,000 based on the inlet diameter and mean bulk inlet velocity) for overall assessment of LES and SGS models for the velocity field. The consistency and the accuracy of the FMDF are established in the next two sections. Comparison with the experimental data of Gould et al. [36,37] is made in the last section.

A. Nonreacting Dump-Combustor Simulations

The experimental setup, the geometry of the simulated dump combustor and the multiblock grid system employed in one of our nonreacting LES calculations for the case with the added inlet nozzle are shown in Fig. 4. All grids are generated by using transfinite interpolation with controls for clustering, smoothness, and orthogonality [103,104]. The centerline singularity associated with O–H grids is eliminated by using an H–H grid in the center of the duct. To have an overlap between the H–H and the O–H grids, we needed to add an extra grid point at every corner. By adding these points, the skewness problem at corners is essentially eliminated. In fact, the skewness or orthogonality at those corner points are comparable to cells in the H–H grid. Grid clustering is used in the regions near the walls, in the shear layer, and close to the inlet. Different cases with various grid resolutions, SGS stress models, inflow velocity, and boundary conditions are considered.

Figure 5 shows the radial variations of the mean (time-averaged) filtered axial velocity for the reference case at several axial locations as obtained by LES with various SGS stress models. The predicted root mean square (RMS) values of the axial velocity by LES are compared with the experimental data in Fig. 6. The Smagorinsky

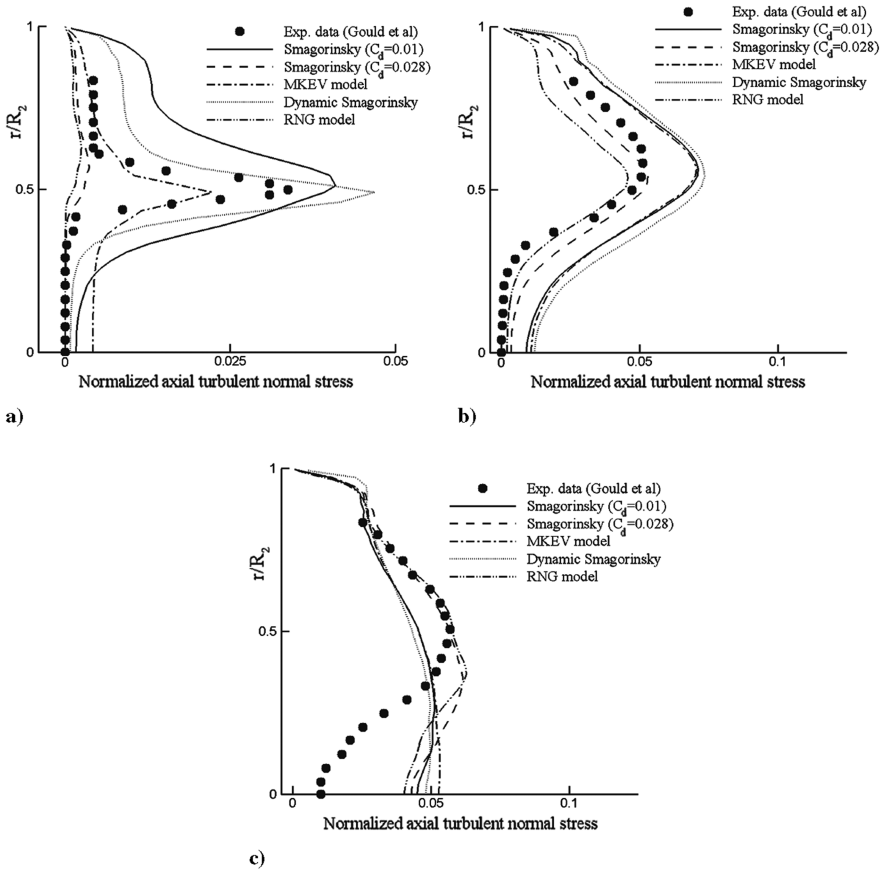

Fig. 6 Comparison between LES with different SGS models and experiment at various axial locations for normal axial turbulent stress, a) $x/H = 1$, b) $x/H = 4$, and c) $x/H = 8$. The LES calculations are for the case without the inlet nozzle.

[60,61], MKEV [11], dynamic Smagorinsky [62–64], and algebraic RNG [65] SGS closures are implemented. For the reference case, the grid resolution is $159 \times 47 \times 58$ for the interior block and $159 \times 17 \times 17$ for the outer block. The results reported in Figs. 5 and 6 are for the case without the inlet nozzle; only the flow inside the combustor is simulated. Evidently, the mean velocities obtained by the Smagorinsky model with a higher Smagorinsky coefficient and also those with the RNG model compare reasonably well with the experimental data at locations far away from the inlet. However, close to inlet the dynamic Smagorinsky model yields slightly better results. The predicted RMS values of the filtered axial velocity also do not suggest that any of the tested SGS stress models are significantly better than the others. The reattachment point predicted by LES with various models is between 7.5–7.9 step heights, which is slightly lower than the experimental value (8.0 step heights).

In this work, the effects of inlet- and outlet-boundary conditions have been extensively studied. Again, all simulations are conducted without the inlet nozzle and only compute the flow within the combustor. Various boundary conditions that satisfy the physical and mathematical criteria are considered. The results of our numerical experiments show that for outflow, the characteristic boundary condition coupled with the convective boundary condition is stable. For the inlet boundary condition, experimental data were used to generate turbulent perturbations for all velocity components, and the mean velocities are set to be the same as the experiment. Basic features of the five tested boundary conditions at dump-combustor inlet (INBC) are summarized in the following list:

1) INBC 1: $T = cte$, characteristic boundary condition is used to compute the density [83] and pressure is computed through the equation of state.

2) INBC 2: $T = cte$, the density is allowed to float via pseudo-characteristic boundary condition, $\partial\rho/\partial x = 0$ or $\partial^2\rho/\partial x^2 = 0$, and pressure is computed through the equation of state.

3) INBC 3: $T = cte$, the pressure is allowed to float via pseudocharacteristic boundary condition,$\partial\rho/\partial x = 0$ or $\partial^2\rho/\partial x^2 = 0$, and the density is computed through the equation of state.

4) INBC 4: The temperature is allowed to float at the inlet ($\partial T/\partial x = 0$), the pressure is kept constant and the density is computed through the equation of state.

5) INBC 5: The temperature is allowed to float at the inlet ($\partial T/\partial x = 0$), the density is kept constant, and the pressure is computed through the equation of state.

Our simulations indicate that INBC 1, 2, and 3 are causing some numerical instability at long times. In all the other tested boundary conditions that are based on fixed temperature, the instability

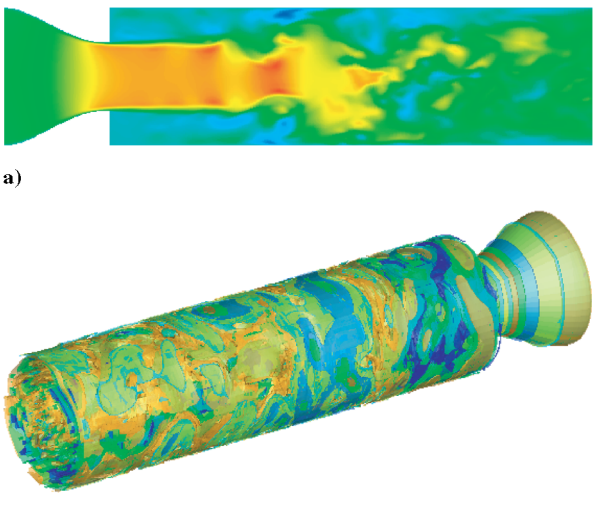

Fig. 7 a) Contours of the instantaneous axial velocity at $z = 0$ plane, and b) isosurfaces of the vorticity magnitude, for the case with nozzle.

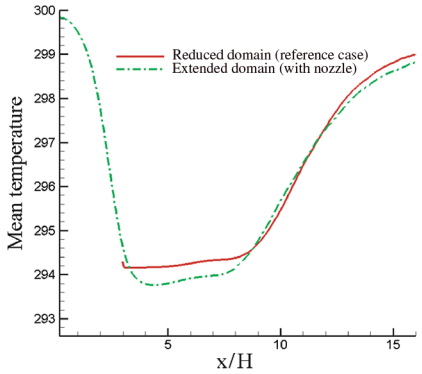

Fig. 8 Axial variations of the centerline temperature in the dump combustor for cases with and without the inlet nozzle.

problem seems to persist. When the computational domain is cut off right at the sudden-expansion point and the temperature is fixed, the imposed boundary condition cannot adjust to the changes in the interior points and INBC 1, 2, and 3 become ultimately unstable. However, INBC 4 and 5 (which allow the temperature to float) do not exhibit any instability. Here, we use the INBC 5, which yields good results consistent with previous observations [105]. Also, to better understand and eliminate the source of instability, a nozzle similar to that in the experiment was added to the computational domain just before the sudden-expansion point (see Fig. 4). For the simulation

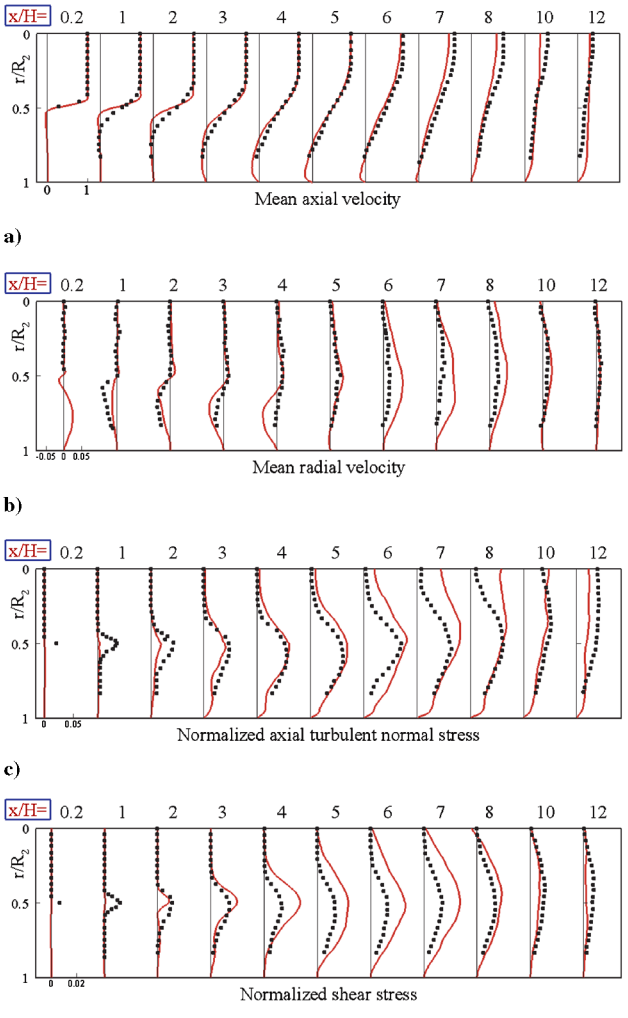

Fig. 9 Radial variations of different turbulent statistics at different axial locations for the case with the inlet nozzle (●, experiment; solid lines, LES).

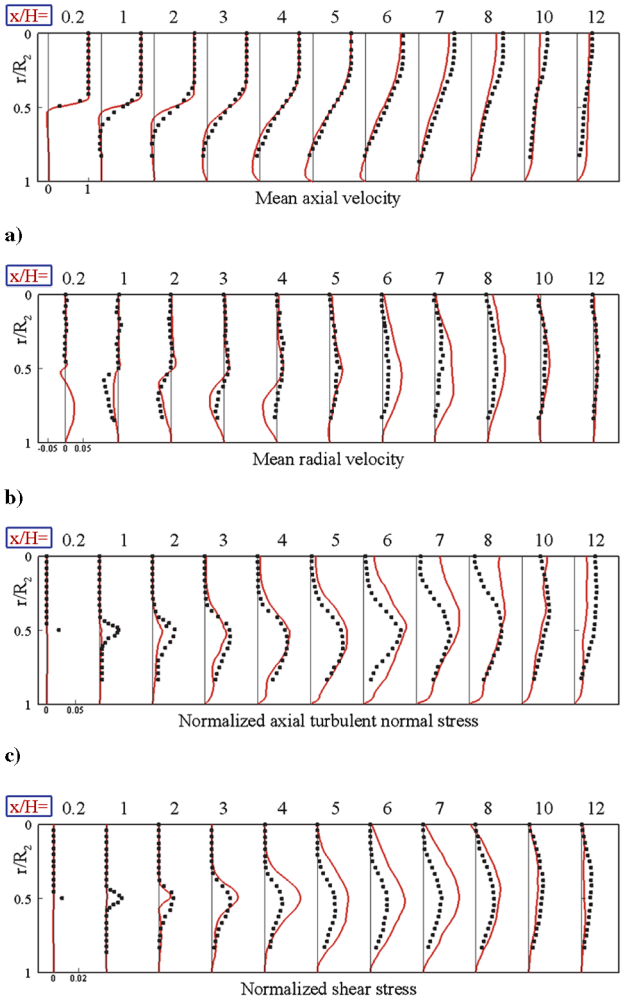

Fig. 10 Radial variations of different turbulent statistics at different axial locations for the high-resolution case (●, experiment; solid lines, LES).

with nozzle, a three-block, O–H grid with the corresponding resolutions of 207 × 17 × 58, 207 × 17 × 17, and 159 × 32 × 58 for different blocks (the resolution is the same in radial and azimuthal direction as compared to the case without nozzle) is employed. Figure 7 shows the contours of instantaneous axial velocity and vorticity magnitude isosurfaces in the dump combustor for the case with the nozzle. Also, Fig. 8 compares the mean centerline temperatures for cases with and without the inlet nozzle. Evidently, the results obtained with and without the nozzle are in good overall

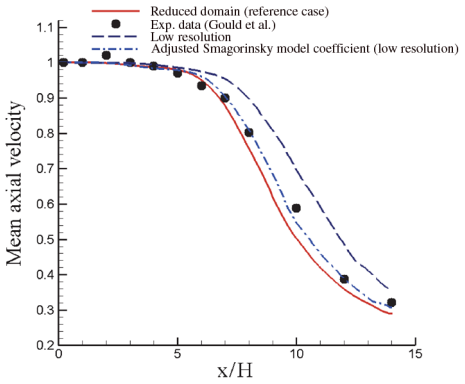

Fig. 11 Axial variations of the centerline velocity in the dump combustor for different cases.

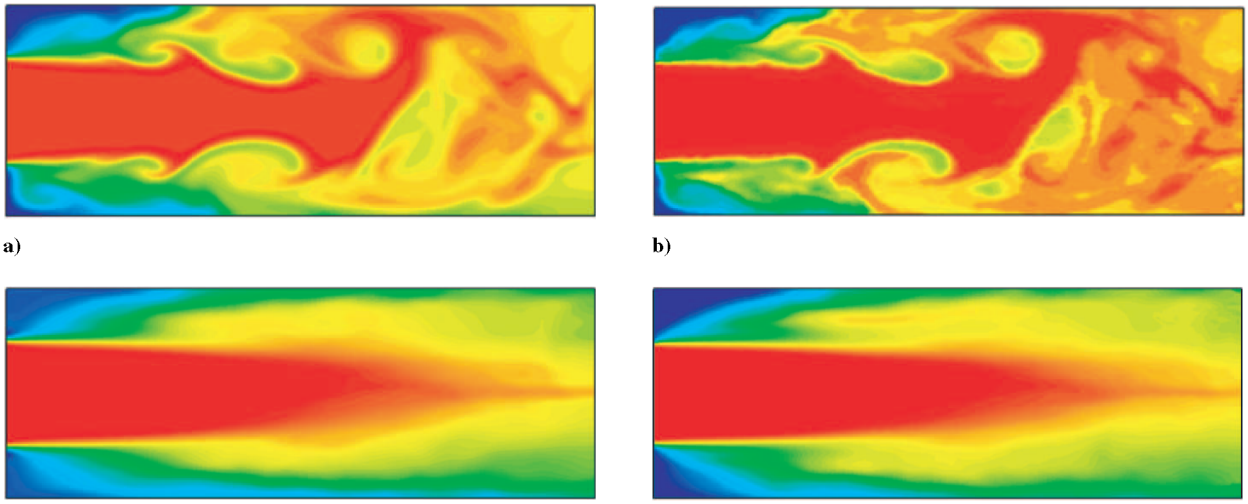

Fig. 12 Contours of the instantaneous and time-averaged conserved scalar in the isothermal nonreacting axisymmetric dump combustor as obtained from the Monte Carlo and finite-difference data, a) instantaneous FD values, b) instantaneous MC values, c) time-averaged FD values, and d) time-averaged MC values.

agreement. This suggests that the boundary condition used for temperature in the case without nozzle is accurate and allows correct adjustment of boundary values to the flow inside the dump combustor. The results also correctly indicate that the temperature continuously decreases as the flow passes through the nozzle. Fixing the temperature at the inlet for the case without the nozzle causes some errors, as expected. The same results were obtained for the case with the nozzle using the characteristic boundary at the inlet and using the pseudocharacteristic boundary condition for the pressure or the density [83]. In Fig. 9, the predicted mean axial velocity, mean radial velocity, normalized axial turbulent normal stress, and normalized shear stress by LES for the case with the nozzle have been compared with the experimental data at different downstream locations. The predicted velocity profile at $x/H = 0.2$ is in good agreement with the experimental data. As expected, the nozzle generates a nearly flat profile with a very thin shear layer at the combustor inlet. The mean axial velocity predictions are almost the same as those in previous (reference) case without the nozzle. However, the agreement with the experiment is better for the mean radial velocity and other turbulence statistics. As mentioned earlier, the numerical error due to the inlet boundary condition is less significant when the flow in the nozzle is also simulated.

To assess the dependency of the results to grid resolution, various simulations with different grid layouts and resolutions are considered. This is a complex issue for LES because the limit of LES is DNS. Here, we want to ensure that the flow statistics are not very sensitive to grid resolution. Our results show that the resolved flow variables are indeed accurately computed by LES provided that the residual or SGS correlations are properly modeled. The sensitivity of results to grid resolution, particularly the results at shear layer is discussed later in the paper. We have considered several different simulations with different grid resolutions. The results for the reference case indicate that around 5–20% of the total turbulent energy is in the SGS range, depending on the location. This implies that the grid resolution is acceptable according to the arguments made by Pope [106]. We also assess the accuracy by comparing the computed results with the experimental data for low- and high-grid resolutions. Both mean and RMS values are compared with the experimental data, and good agreement is obtained. The results for higher grid resolution ($159 \times 61 \times 66$ and $159 \times 19 \times 19$) are

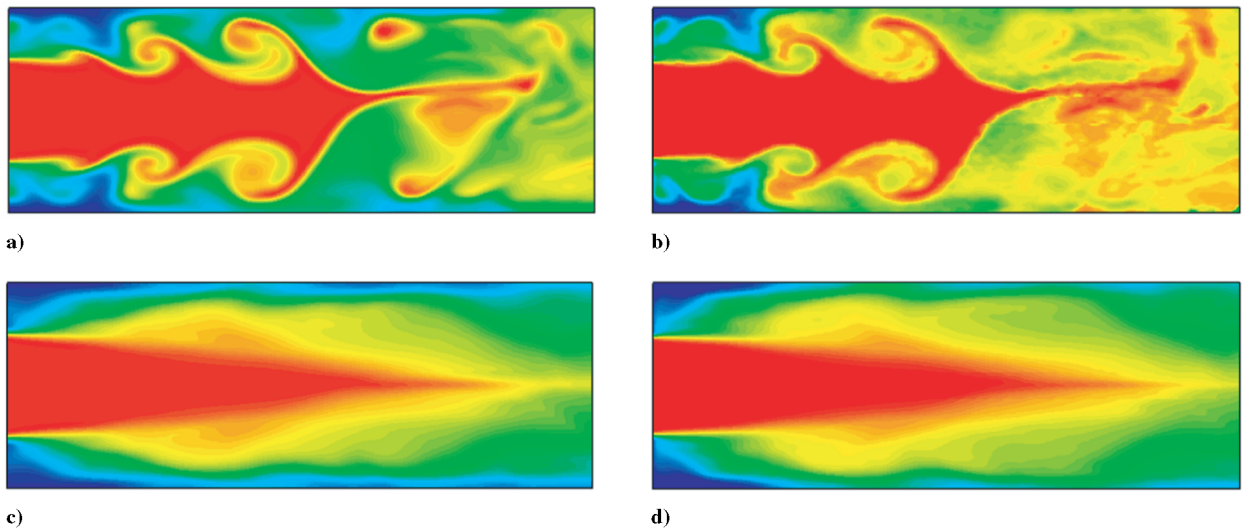

Fig. 13 Contours of the instantaneous and time-averaged values of the filtered conserved scalar in the nonisothermal nonreacting axisymmetric dump combustor as obtained by LES/FMDF, a) instantaneous FD values, b) instantaneous MC values, c) time-averaged FD values, and d) time-averaged MC values.

compared with the experimental data in Fig. 10. A simulation with lower grid resolution ($155 \times 35 \times 42$ and $155 \times 13 \times 13$), as compared to the reference case, is also performed. The comparison between the results shown in Fig. 10 with those in Fig. 9 indicates that although the grid resolution effects are not very significant; there are some discrepancies between the results obtained with various resolutions/grid layouts. However, the discrepancies are not just due to grid resolution, rather they are mainly due to the SGS stress model. For example in the Smagorinsky closure, the modeled SGS stress is directly dependent to the cell size and can be overestimated for larger cell sizes. To show that the discrepancy between the low-resolution and high-resolution results is mainly caused by the SGS model, another simulation with a different Smagorinsky model coefficient was conducted. In this new simulation, the Smagorinsky model coefficient was adjusted so that for the cells in the shear layer zone the magnitude of $C_d\Delta^2$ is nearly the same as that in the reference case. As observed in Fig. 11, the centerline velocity for the new low-resolution case with the adjusted Smagorinsky coefficient is very close to that for the reference case and experiment. Without the model coefficient adjustment, the centerline velocity in the low-resolution case does not decay as fast as that in the reference case, simply because the local filter size in the Smagorinsky model is bigger. In other words, the turbulent viscosity is overestimated in the shear layer by the Smagorinsky model, resulting in slower growth in the turbulence and a slower decay rate of the centerline velocity.

B. Nonreacting Simulations—Consistency of FMDF

The objective of the results presented in this section is to demonstrate the consistency of the FMDF and its Lagrangian–MC scheme with the conventional LES models and FD method for nonreacting flows. For this, the filtered temperature and conserved scalar variables as calculated by LES/FD and FMDF/MC models are compared. Both isothermal and nonisothermal cases are considered. The nonreacting isothermal dump-combustor simulations considered here are similar to those reported in the preceding section. However, here the FMDF equation and an additional finite-difference equation for a conserved (passive) scalar are solved. The normalized scalar value is initially zero but is set to 1.0 at the combustor inlet. Figure 12 shows the contours of the instantaneous and mean conserved scalar at relatively long time as obtained by LES/FD and FMDF/MC. The MC and FD variables are obtained from the Monte Carlo particles and finite-difference grid points. The results in Fig. 12 show that the turbulent scalar mixing process is similarly captured by the two models, indicating an excellent consistency between the FD and MC predictions. The time-averaged scalar values also suggest that FD and MC are consistent at all times. Expectedly, there is no significant temperature/density variations in the simulated isothermal nonreacting flow. Nevertheless, it is possible to calculate the filtered temperature from the LES/FD and FMDF/MC data and establish the consistency between the predicted temperatures by these methods. Our results (not shown) indeed indicate that the computed instantaneous and mean temperature fields by the MC and FD methods are very close, even though the maximum temperature difference in the flow is about 3% of the ambient temperature.

To further establish the consistency and the accuracy of the LES/FD and FMDF/MC methods, a more complex nonisothermal nonreacting case is considered. In this case, the variations in flow density and temperature are significant, as the temperature is set to be $2T_0$ ($T_0 = 300$ K) at combustor inlet, whereas it is initially T_0 elsewhere. However, the pressure variations remain small at all times. Figure 13 shows a comparison between the MC and FD scalar values in the nonisothermal case. In this case, the scalar initialization and inlet conditions are the same as those in the isothermal case, but the temperature/density effects on molecular and turbulent mixing are significant. For one, the molecular diffusivity coefficient varies with the temperature. Also, the density variations at the shear layer changes the instability of the layer and subsequently the turbulence mixing. Nevertheless, the data indicates a very good consistency between the results obtained by the FD and MC methods. The planar instantaneous and mean temperature contours in Fig. 14 also show a very good consistency between Eulerian LES/FD and Lagrangian FMDF/MC results. This again suggests that the finite difference and Monte Carlo solvers are both reliable and accurate. In addition to scalar and temperature, we also compared the FMDF/MC and LES/FD densities. Our results for the densities (not shown) also indicate a good consistency between the FMDF/MC and LES/FD results. In the FMDF method, the density is calculated based on the weighting of the particles located in the ensemble domain (control-volume cell) by averaging over the particles. The LES/FD density is the filtered density at the Eulerian grid points.

C. Reacting Simulations—Accuracy of LES/FMDF

In this section, the numerical data obtained by LES/FMDF for the reacting case are compared with the experimental data [37]. As mentioned before, the reaction for the lean-premixed propane-air mixture with the equivalence ratio of 0.5 is modeled with a one-step global reaction mechanism [76]. The flow Reynolds number, based on inlet diameter and mean bulk inlet velocity, is 115,000. The simulations are performed with the reference (nonreacting case) grid resolutions of $159 \times 47 \times 58$ for the interior block and $159 \times 17 \times 17$ for the outer block. Figure 15 shows the 3-D isolevels of vorticity

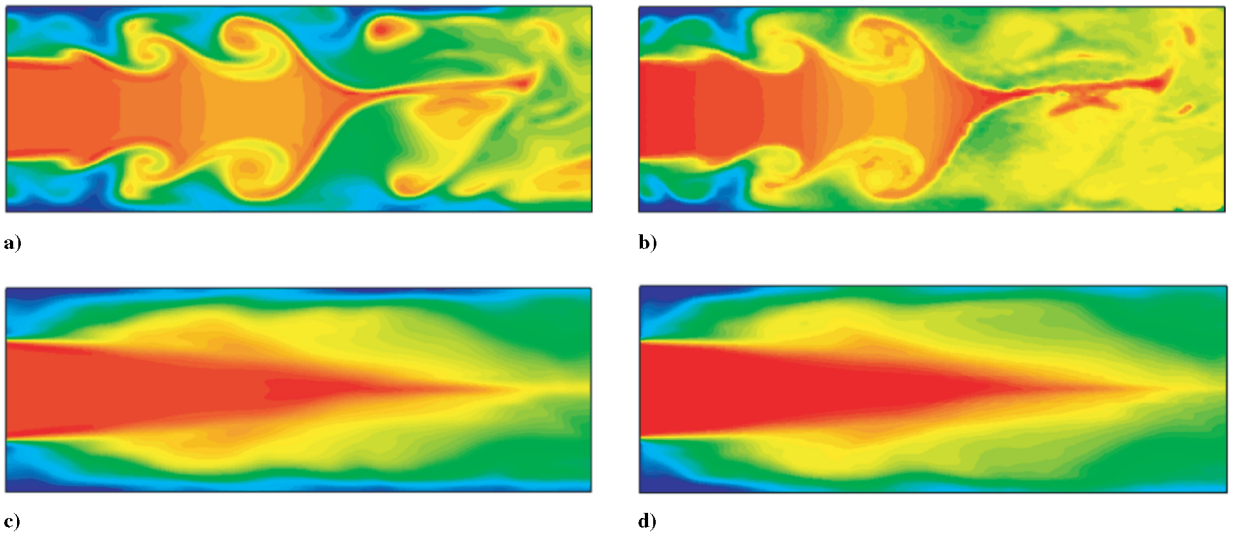

Fig. 14 Contours of the instantaneous and time-averaged values of the filtered temperature in the nonisothermal nonreacting axisymmetric dump combustor as obtained by LES/FMDF, a) instantaneous FD values, b) instantaneous MC values, c) time-averaged FD values, and d) time-averaged MC values.

magnitude and the Monte Carlo particle distribution, and the 2-D contours of fuel and heat release for the reacting case. As Figs. 15b and 15c indicate, a significant amount of unburned fuel and oxidant exit the domain, which is consistent with the experiment [37]. The mean axial velocity contours (not shown) indicate that the recirculation zone (defined by the streamline with zero mean axial velocity) is thinner and shorter in the reacting case, mainly due to volumetric expansion in the radial direction. Further investigation for other flow conditions indicate that by increasing the inflow turbulence one can significantly enhance the combustion efficiency in the combustor.

As mentioned before, the consistency between LES/FD and FMDF/MC methods can only be established for nonreacting flows because the nonlinear reaction source/sink terms are closed in the FMDF equations but have to be modeled in the conventional FD equations. However, one can calculate these source/sink terms from the Monte Carlo particles and FMDF model and use them in the LES/FD equations. By doing this, one can examine the consistency between LES/FD and FMDF/MC in reacting flows provided that MC values of the reaction terms are available. Figure 16 shows the MC and FD values of the instantaneous and mean filtered temperatures at different downstream locations. As indicated before, in any of our hybrid simulations (reacting and nonreacting) the filtered temperature is a redundant variable that can be obtained from both the Monte Carlo particles and finite-difference grids. Evidently, the values obtained by the Eulerian FD and Lagrangian–MC methods are very close, indicating a good consistency between the two methods in the reacting case.

Figures 17 and 18 show the comparison between LES/FMDF and experimental results for mean axial velocity and mean temperature at different axial locations. The LES/FMDF results are obtained for the reference case. Despite a reasonably good overall agreement between the numerical and experimental data, the LES/FMDF predictions do not fully match with the experiment for the reasons explained later. As the results in Fig. 17 suggest, the reacting-flow centerline velocity does not decay nearly as fast as the cold-flow centerline velocity. This is due to low-pressure gradient at the centerline and slower growth of shear layer in the reacting case. Higher mean axial velocities in the shear layer in the reacting case are due in part to combustion-induced volumetric flow expansion. In the reacting case, the core region of the flow stays relatively cool and the maximum temperatures are achieved in the recirculation zone and near to the developing boundary layer downstream of the reattachment point. Figure 17 shows that the computed mean axial velocity is slightly higher than the measured velocity at shear layer. This could be due to boundary conditions at the combustor inlet.

To examine the effects of the boundary conditions, a nozzle similar to that in experiment was added to the computational domain, right before the combustor. For this case, the consistency between Eulerian and Lagrangian data (Fig. 19) again indicates that the FMDF results are reliable. The fuel mass fraction contours in Fig. 20 indicate that the flow and combustion behaviors in the case with the added nozzle are in general similar to those in the case without the nozzle. However, Fig. 21 shows that the predicted mean axial velocity by LES/FMDF compares better with the experiment particularly in the shear layer zone. This suggests that the discrepancy between the predicted and measured values in the shear layer in the case without nozzle is primarily due to inlet boundary condition. Figure 22 compares the mean temperature profiles with the experimental data, for the case with nozzle. Clearly, by adding the nozzle to the computational domain the LES/FMDF predictions of mean temperature improves as well. The maximum, normalized temperature in this simulation is approximately five times of the ambient temperature. The effect of the outlet boundary does not seem to be very significant as long as the flow and pressure oscillations are allowed to exit the computational domain.

Overall, our numerical results are consistent with the experiment and correctly exhibit some of the interesting features of the flowfield and combustion in the dump combustor. For example, the axial pressure gradient at centerline in the reacting-flow case is approximately four times less than that in the cold-flow case. This is consistent with the momentum balance and is due to increased velocity (and temperature) in the shear layer. Our results (not shown) also indicate that the turbulence level is lower in the reacting-flow case over most of the flowfield, possibly indicating either reduced production and/or increased dissipation of the turbulent kinetic energy. The locations of the peak turbulence levels are shifted radially outward, consistent with the location of the dividing streamlines defining the thinner recirculation zone in the reacting flow. The reacting flowfield is more isotropic and the production of turbulence generated by shear is much lower than in the cold flow. Low shear in reacting flow occurs by an increased turbulent dissipation rate (due to the temperature dependent viscosity) and by the volumetric expansion in the reacting flow. The dynamic viscosity increases by a factor of approximately three at the elevated temperature existing in the combustion chamber. Likewise the kinematic viscosity increases by a factor of approximately 15 (because density decreases by a factor of 5) in the combustion chamber. Increased turbulent dissipation may reduce eddy coalescence and structures in reacting flows and shear layers.

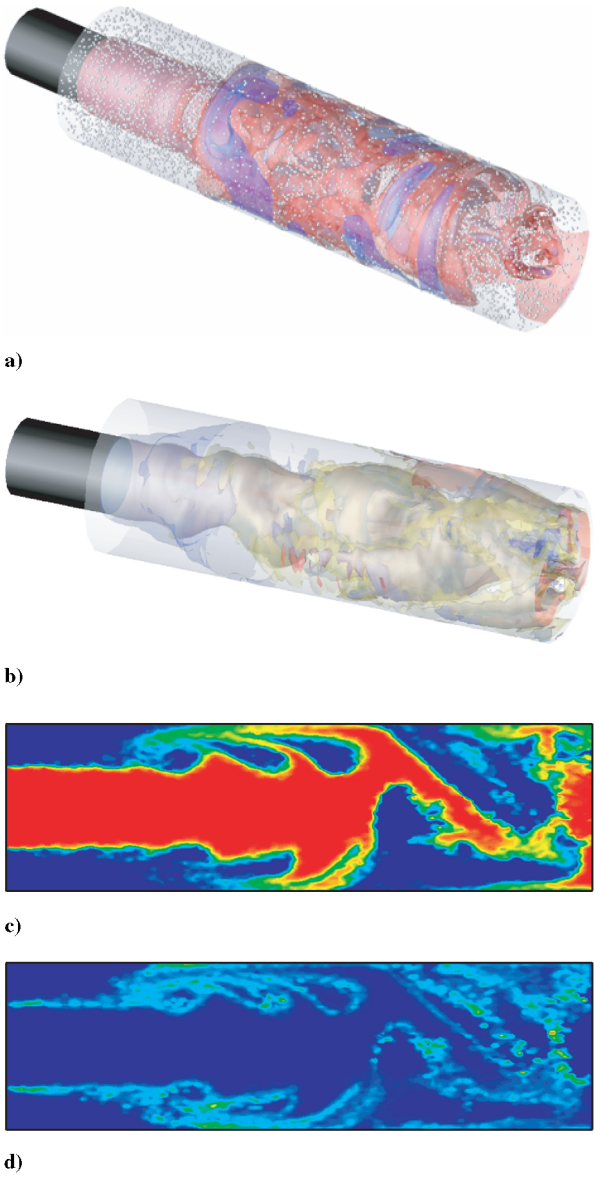

Fig. 15 a) Three-dimensional isolevels of the instantaneous vorticity magnitude and Monte Carlo particles, b) three-dimensional isolevels of the fuel distribution, c) two-dimensional contours of the fuel mass fraction, d) two-dimensional contours of the heat release; in an axisymmetric dump combustor as obtained by LES/FMDF.

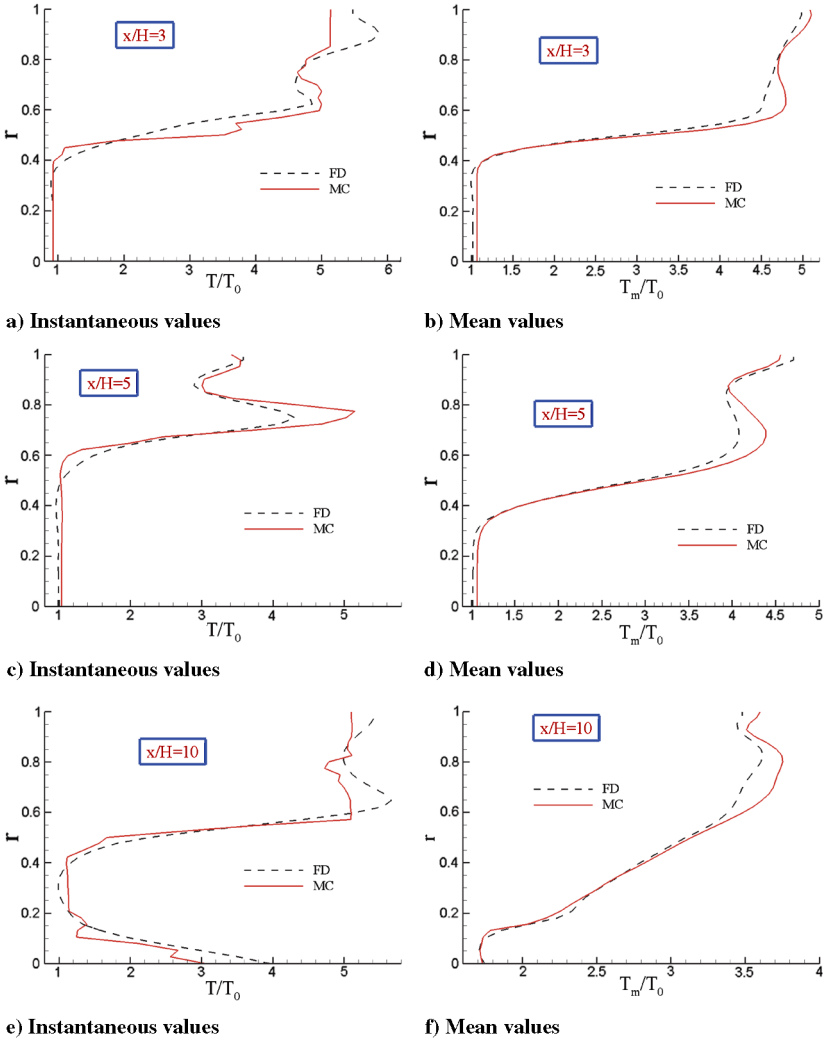

Fig. 16 The instantaneous and mean values of the filtered temperature, obtained from the FD and MC data at different downstream locations.

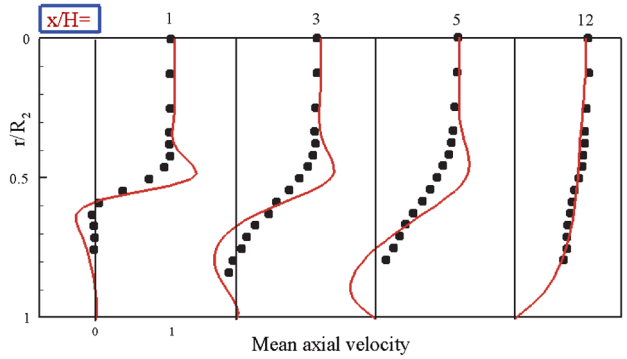

Fig. 17 Radial variations of the mean axial filtered velocity as predicted by the LES/FMDF and compared with the experimental data at different downstream locations (●, experiment; solid lines, LES).

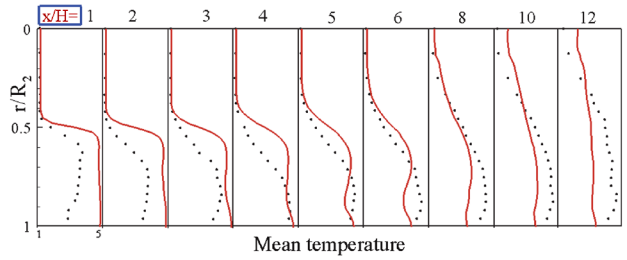

Fig. 18 Radial variations of the mean filtered temperature as predicted by LES/FMDF and compared with the experimental data at different downstream locations (●,experiment; solid lines, LES).

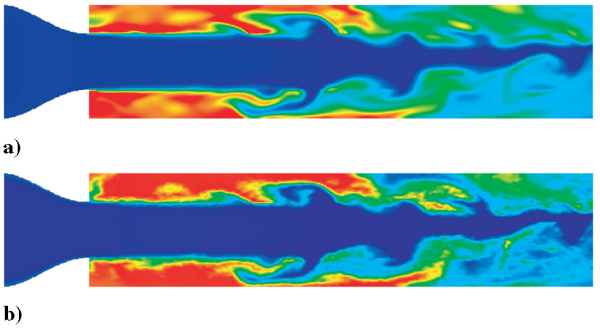

Fig. 19 Two-dimensional contours of the instantaneous filtered temperature in the reacting case with the inlet nozzle as obtained by the LES/FMDF, a) FD values, b) MC values.

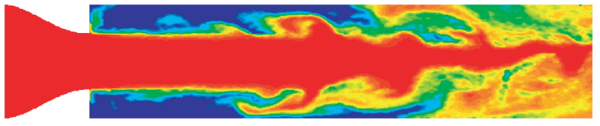

Fig. 20 Two-dimensional contours of the fuel mass fraction as obtained by LES/FMDF for the reacting case with the inlet nozzle.

V. Conclusions

A hybrid Eulerian–Lagrangian numerical methodology is developed and implemented for large-eddy simulation of turbulent reacting flows in generalized coordinate systems. The Eulerian numerical/mathematical model is based on a high-order,

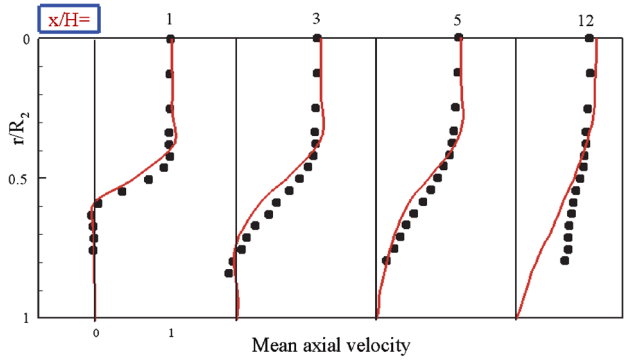

Fig. 21 Radial variations of the mean axial filtered velocity as obtained by LES/FMDF for the reacting case with the inlet nozzle and compared with the experimental data (●, experiment; solid lines, LES).

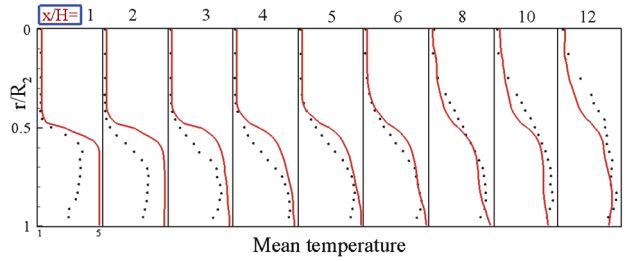

Fig. 22 Radial variations of the mean filtered temperature as obtained by LES/FMDF for the reacting case with the inlet nozzle and compared with the experimental data (●, experiment; solid lines, LES).

compact-differencing formula with multiblock capability and is developed for LES of compressible turbulent nonreacting and reacting flows in complex geometries. The numerical scheme is validated by performing direct and large-eddy simulations of isotropic turbulence, round/planar turbulent jets, and high-Reynolds number turbulent flows in an axisymmetric dump combustor. A detailed investigation of the effects of boundary conditions, subgrid-scale model, and inlet/outlet flow conditions is carried out. A good comparison between our current results and those obtained through other high-order schemes and experiments indicates the accuracy of our numerical technique.

The SGS combustion model is based on the filtered mass density function approach that is extended here for LES of turbulent combustion in complex geometries and is applied to a dump combustor. An efficient algorithm is developed for Lagrangian–Monte Carlo implementation of the FMDF, making the application of FMDF to complex geometries feasible. The new scheme offers much higher computational efficiency than the algorithms previously developed for similar hybrid schemes. The numerical schemes previously developed for unstructured grids are not appropriate for the LES/FMDF, at least major advances are needed before LES/FMDF can be implemented on an unstructured mesh. A comparison between the CPU times associated with our LES/FMDF method on a structured grid with those for RANS/PDF on unstructured grids indicates that our LES/FMDF flow solver is very efficient. The results show that the LES/FD and FMDF/MC are consistent in all tested flow conditions. Additionally, the LES/FMDF results for a reacting flow in a dump combustor show favorable agreement with the experimental data. The numerical predictions were shown to improve by adding an inlet nozzle component to the computational domain, which effectively reduces the negative effects of inlet boundary conditions.

Here, we have developed and tested an efficient and accurate numerical framework for the application of the LES/FMDF, and we have discussed the new results obtained by the model for an important combustion system that has wide applications in gas turbine and ramjet engines. The numerical simulations conducted in this paper indicate that the hybrid Eulerian–Lagrangian LES/FMDF methodology is an affordable, consistent, and reliable methodology for three-dimensional, time-dependent simulations of turbulent flows with large-density variations and strong turbulence-combustion interactions. The LES/FMDF is not, however, a fully accurate model and can benefit from improvements in some of its submodels.

Acknowledgments

This work was sponsored by the U.S. Office of Naval Research under Grant N00014-01-1-0843. Gabriel Roy served as the Program Manager for this grant. Computational resources were provided by the Super Computing Institute for Digital Simulation and Advanced Computation at the University of Minnesota and by the High-Performance Computing Center at the Michigan State University.

References

[1] McMurtry, P. A., Menon, S., and Kerstein, R. A., "A Linear Eddy Sub-Grid Model for Turbulent Reacting Flows: Application to Hydrogen-Air Combustion," *Proceedings of the 24th Symposium (International) on Combustion*, The Combustion Institute, Pittsburgh, PA, 1992, pp. 271–278.

[2] Menon, S., McMurtry, P. A., and Kerstein, A. K., "A Linear Eddy Sugbrid Model of Turbulent Combustion," *Large Eddy Simulations of Complex Engineering and Geophysical Flows*, edited by B. Galperin, and S. A. Orszag, Chap. 14, Cambridge Univ. Press, Cambridge, U.K., 1993, pp. 287–314.

[3] Gao, F., and O'Brien, E. E., "A Large Eddy Scheme for Turbulent Reacting Flows," *Physics of Fluids A*, Vol. 5, No. 6, 1993, pp. 1282–1284.
doi:10.1063/1.858617

[4] Madnia, C. K., and Givi, P., "Direct Numerical Simulation and Large Eddy Simulation of Reacting Homogeneous Turbulence," *Large Eddy Simulations of Complex Engineering and Geophysical Flows*, edited by B. Galperin, and S. A. Orszag, Chap. 15, Cambridge Univ. Press, Cambridge, U.K., 1993, pp. 315–346.

[5] Frankel, S. H., Adumitroaie, V., Madnia, C. K., and Givi, P., "Large Eddy Simulations of Turbulent Reacting Flows by Assumed PDF Methods," *Engineering Applications of Large Eddy Simulations*, edited by S. A. Ragab, and U. Piomelli, Chap. 15, FED-Vol. 162, ASME, New York, 1993, pp. 81–101.

[6] Cook, A. W., and Riley, J. J., "A Subgrid Model for Equilibrium Chemistry in Turbulent Flows," *Physics of Fluids*, Vol. 6, No. 8, 1994, pp. 2868–2870.
doi:10.1063/1.868111

[7] Fureby, C., and Lofstrom, C., "Large-Eddy Simulations of Bluff Body Stabilized Flames," *Proceedings of the 25th Symposium (International) on Combustion*, The Combustion Institute, Pittsburgh, PA, 1994, pp. 1257–1264.

[8] Branley, N., and Jones, W. P., "Large Eddy Simulation of a Turbulent Non-Premixed Flame," *Combustion and Flame*, Vol. 127, Nos. 1–2, Oct. 2001, pp. 1914–1934.
doi:10.1016/S0010-2180(01)00298-X

[9] Cook, A. W., Riley, J. J., and Kosály, G., "A Laminar Flamelet Approach to Subgrid-Scale Chemistry in Turbulent Flows," *Combustion and Flame*, Vol. 109, No. 3, 1997, pp. 332–341.
doi:10.1016/S0010-2180(97)83066-0

[10] Mathey, F., and Chollet, J. P., "Large Eddy Simulation of Turbulent Reactive Flows," *Proceedings of the Eleventh Symposium on Turbulent Shear Flows*, 8–10 Sept. 1997, pp. 16-19–16-24.

[11] Colucci, P. J., Jaberi, F. A., Givi, P., and Pope, S. B., "Filtered Density Function for Large Eddy Simulation of Turbulent Reacting Flows," *Physics of Fluids*, Vol. 10, No. 2, 1998, pp. 499–515.
doi:10.1063/1.869537

[12] DesJardin, P. E., and Frankel, S. H., "Large Eddy Simulation of a Turbulent Nonpremixed Reacting Jet: Application and Assessment of Subgrid-Scale Combustion Models," *Physics of Fluids*, Vol. 10, No. 9, 1998, pp. 2298–2314.
doi:10.1063/1.869749

[13] Jaberi, F. A., and James, S., "A Dynamic Similarity Model for Large Eddy Simulation of Turbulent Combustion," *Physics of Fluids*, Vol. 10, No. 7, 1998, pp. 1775–1777.
doi:10.1063/1.869696

[14] Réveillon, J., and Vervisch, L., "Subgrid-Scale Turbulent Micro-

mixing: Dynamic Approach," *AIAA Journal*, Vol. 36, No. 3, 1998, pp. 336–341.
[15] Jaberi, F. A., Colucci, P. J., James, S., Givi, P., and Pope, S. B., "Filtered Mass Density Function For Large Eddy Simulation of Turbulent Reacting Flows," *Journal of Fluid Mechanics*, Vol. 401, Dec. 1999, pp. 85–121. doi:10.1017/S0022112099006643
[16] Ghosal, S., and Moin, P., "The Basic Equations for the Large Eddy Simulation of Turbulent Flows in Complex Geometry," *Journal of Computational Physics*, Vol. 118, No. 1, April 1995, pp. 24–37. doi:10.1006/jcph.1995.1077
[17] Meneveau, C., and Katz, J., "Scale-Invariance and Turbulence Models for Large-Eddy Simulations," *Annual Review of Fluid Mechanics*, Vol. 32, Jan. 2000, pp. 1–32. doi:10.1146/annurev.fluid.32.1.1
[18] Sagaut, P., *Large Eddy Simulation for Incompressible Flows*, Springer–Verlag, New York, 2001.
[19] Poinsot, T., and Veynante, D., *Theoretical and Numerical Combustion*, 2nd ed., R.T. Edwards, Philadelphia, PA, 2005.
[20] Candel, S., Thevenin, D., Darabiha, N., and Veynante, D., "Progress in Numerical Combustion," *Combustion Science and Technology*, Vol. 149, Dec. 1999, pp. 297–337. doi:10.1080/00102209908952110
[21] Pitsch, H., and Steiner, H., "Large Eddy Simulation of a Turbulent Piloted Methane/Air Diusion Flame (Sandia Flame D)," *Physics of Fluids*, Vol. 12, No. 10, 2000, pp. 2541–2554. doi:10.1063/1.1288493
[22] Collin, O., Ducros, F., Veynate, D., and Poinsot, T., "A Thickened Flame Model for Large Eddy Simulation of Turbulent Premixed Combustion," *Physics of Fluids*, Vol. 12, No. 7, 2000, pp. 1843–1863. doi:10.1063/1.870436
[23] Jiménez, J., Liñán, A., Rogers, M. M., and Higuera, F. J., "A Priori Testing of Subgrid Models for Chemically Reacting Non-Premixed Turbulent Shear Flows," *Journal of Fluid Mechanics*, Vol. 349, Oct. 1997, pp. 149–171. doi:10.1017/S0022112097006733
[24] Cook, A. W., and Bushe, W. K., "A Subgrid-Scale Model for the Scalar Dissipation Rate in Nonpremixed Combustion," *Physics of Fluids*, Vol. 11, No. 3, 1999, pp. 746–749. doi:10.1063/1.869945
[25] Jiménez, J., Ducros, F., Cuenot, B., and Bedat, B., "Subgrid Scale Variance and Dissipation of a Scalar Field in Large Eddy Simulations," *Physics of Fluids*, Vol. 13, No. 6, 2001, pp. 1748–1754. doi:10.1063/1.1366668
[26] Lu, L., Ren, Z., Raman, V., Pope, S. B., and Pitsch, H., "LES/FDF/ISAT Computations of Turbulent Flames," *Proceedings of the 2004 Summer Program, Center for Turbulence Research, NASA Ames Research Center*, Stanford Univ., Stanford, CA, 2004, pp. 283–294.
[27] Cha, C. M., and Troullet, P., "A Subgrid-Scale Mixing Model for Large-Eddy Simulations of Turbulent Reacting Flows Using the Filtered Density Function," *Physics of Fluids*, Vol. 15, No. 6, 2003, pp. 1496–1504. doi:10.1063/1.1569920
[28] Wang, D., Tong, C., and Pope, S. B., "Experimental Study of Velocity Filtered Joint Density Function For Large Eddy Simulation," *Physics of Fluids*, Vol. 16, No. 10, 2004, pp. 3599–3613. doi:10.1063/1.1776194
[29] Subramaniam, S., and Haworth, D. C., "A Probability Density Method for Turbulent Mixing and Combustion on Three-Dimensional Unstructured Deforming Meshes," *International Journal of Engine Research*, Vol. 1, No. 2, 2000, pp. 171–190. doi:10.1243/1468087001545128
[30] Zhang, Y. Z., and Haworth, D. C., "A General Mass Consistency Algorithm for Hybrid Particle/Finite volume PDF Methods," *Journal of Computational Physics*, Vol. 194, No. 1, Feb. 2004, pp. 156–193. doi:10.1016/j.jcp.2003.08.032
[31] Afshari, A., "Large-Scale and High Performance Computations of Complex Turbulent Reacting Flows," Ph.D. Thesis, Michigan State University, East Lansing, MI, Aug. 2006.
[32] Mehravaran, K., "Mathematical Modeling and Numerical Simulations of Chemically Reacting Turbulent Jets," Ph.D. Thesis, Michigan State University, East Lansing, MI, June 2005.
[33] Afshari, A., Almeida, T., Mehravaran, K., and Jaberi, F. A., "Large Scale Simulations of Turbulent Combustion and Propulsion Systems," *Proceedings of the Seventeen ONR Propulsion Meeting,* , June 2004.
[34] Givi, P., "Sugrid Scale Modeling in Turbulent Combustion: A Review," AIAA Paper 2003-5081, July 2003.
[35] Givi, P., "Filtered Density Function for Subgrid Scale Modeling of Turbulent Combustion," *AIAA Journal*, Vol. 44, No. 1, 2006, pp. 16–23.
[36] Gould, R. D., Stevenson, W. H., and Thompson, H. D., "Investigation of Turbulent Transport in an Axisymmetric Sudden Expansion," *AIAA Journal*, Vol. 28, No. 2, 1990, pp. 276–283.
[37] Gould, R. D., Stevenson, W. H., and Thompson, H. D., "Simultaneous Velocity and Temperature Measurements in a Premixed Dump Combustor," *Journal of Propulsion and Power*, Vol. 10, No. 5, 1994, pp. 639–645.
[38] Dellenback, P. A., Metzger, D. E., and Neitzel, G. P., "Measurements in Turbulent Swirling Flow Through an Abrupt Axisymmetric Expansion," *AIAA Journal*, Vol. 26, No. 6, 1988, pp. 669–681.
[39] Stieglmeier, M., Tropea, C., Weiser, N., and Nitsche, W., "Experimental Investigation of the Flow Through Axisymmetric Expansions," *Journal of Fluids Engineering*, Vol. 111, Dec. 1989, pp. 464–471.
[40] Ahmed, S. A., and Nejad, A. S., "Premixed, Turbulent Combustion of Axisymmetric Sudden Expansion Flows," *International Journal for Heat and Fluid Flow*, Vol. 13, No. 1, 1992, pp. 15–21.
[41] Cole, D. R., and Glauser, M. N., "Flying Hot Wire Measurements in an Axisymmetric Sudden Expansion," *Journal of Experimental Thermal and Fluid Science*, Vol. 18, No. 2, Oct. 1998, pp. 150–167.
[42] Lieuwen, T., and Zinn, B. T., "On the Experimental Determination of Combustion Process Driving in an Unstable Combustor," *Combustion Science and Technology*, Vol. 157, No. 1, 2000, pp. 111–127. doi:10.1080/00102200008947312
[43] Sommerfeld, M., and Qiu, H.-H., "Experimental Studies of Spray Evaporation in Turbulent Flow," *International Journal for Heat and Fluid Flow*, Vol. 19, No. 1, Feb. 1998, pp. 10–22.
[44] Sommerfeld, M., and Qiu, H.-H., "Detailed Measurements in a Swirling Particulate Two-Phase Flow by a Phase-Doppler Anemometer," *International Journal for Heat and Fluid Flow*, Vol. 12, No. 1, 1991, pp. 20–28.
[45] Chuang, S.-H., Lin, H.-C., Tai, F.-M., and Sung, H.-M., "Hot Flow Analysis of Swirling Sudden Expansion Dump Combustor," *International Journal for Numerical Methods in Fluids*, Vol. 14, No. 2, Jan. 1992, pp. 217–239. doi:10.1002/fld.1650140208
[46] Guo, B., Langrish, T. A. G., and Fletcher, D. F., "Simulation of Turbulent Swirl Flow in an Axisymmetric Sudden Expansion," *AIAA Journal*, Vol. 39, No. 1, 2001, pp. 96–102.
[47] Zhang, H. Q., Chan, C. K., and Lau, K. S., "Numerical Simulation of Sudden Expansion Particle Laden Flows Using an Improved Stochastic Separated Flow Model," *Numerical Heat Transfer, Part A: Applications*, Vol. 40, No. 1, July 2001, pp. 89–102.
[48] Chuang, S.-H., Yang, C.-H., and Wu, N.-J., "Predictions of Swirling Flow in Sudden Expansion Dump Combustor with Flameholder Side Inlet Using Two-Step Combustion Model," *International Journal of Numerical Methods for Heat and Fluid Flow*, Vol. 9, No. 7, 1999, pp. 764–787. doi:10.1108/09615539910291154
[49] Dailey, L., Simons, T. A., and Pletcher, R. H., "Large Eddy Simulation of Isotropic Decaying Turbulence with Structured and Unstructured Grid Finite Volume Methods," FED-Vol. 242, *Proceedings of the ASME Fluids Engineering Division*, 1996, pp. 245–252.
[50] Schlüter, J. U., Pitsch, H., and Moin, P., "Consistent Boundary Conditions for Integrated LES/RANS Simulations: LES Outow Conditions," AIAA Paper 02-3121, June 2002.
[51] Huang, Y., Sung, H.-G., Hsieh, H.-Y., and Yang, V., "Large Eddy Simulation of Combustion Dynamics of Lean Premixed Swirl Stabilized Combustor," *Journal of Propulsion and Power*, Vol. 19, No. 5, 2003, pp. 782–794.
[52] Moin, P., and Apte, V., "Large-Eddy Simulation of Realistic Gas Turbine Combustors," *AIAA Journal*, Vol. 44, No. 4, 2006, pp. 698–708.
[53] Visbal, M. R., and Gaitonde, D. V., "High-Order-Accurate Methods for Complex Unsteady Subsonic Flows," *AIAA Journal*, Vol. 37, No. 10, 1999, pp. 1231–1239.
[54] Visbal, M. R., and Gaitonde, D. V., "Pade Type High-Order Boundary Filters for the Navier–Sotkes Equations," *AIAA Journal*, Vol. 38, No. 11, 2000, pp. 2103–2112.
[55] Pulliam, T. H., and Steger, J. L., "Implicit Finite-Difference Simulations of Three-Dimensional Compressible Flow," *AIAA Journal*, Vol. 18, No. 2, 1980, pp. 159–167.
[56] Vinokur, M., "Conservation Equations of Gas Dynamics in Curvilinear Coordinate Systems," *Journal of Computational Physics*, Vol. 14, No. 2, Feb. 1974, pp. 105–125. doi:10.1016/0021-9991(74)90008-4
[57] Steger, J. L., "Implicit Finite-Difference Simulation of Flow About Arbitrary Two-Dimensional Geometries," *AIAA Journal*, Vol. 16, No. 7, 1978, pp. 679–686.

[58] Anderson, D. A., Tannehill, J. C., and Pletcher, R. H., *Computational Fluid Mechanics and Heat Transfer*, McGraw–Hill, New York, 1984.
[59] Aldama, A. A., *Filtering Techniques for Turbulent Flow Simulations*, Vol. 49, Lecture Notes in Engineering, Springer–Verlag, New York, 1990.
[60] Smagorinsky, J., "General Circulation Experiments with the Primitive Equations. 1. The Basic Experiment," *Monthly Weather Review*, Vol. 91, No. 3, 1963, pp. 99–164. doi:10.1175/1520-0493(1963)091<0099:GCEWTP>2.3.CO;2
[61] Yoshizawa, A., "Statistical Theory for Compressible Turbulent Shear Flows, with the Application to Subgrid Modelling," *Physics of Fluids*, Vol. 29, No. 7, 1986, pp. 2152–2164. doi:10.1063/1.865552
[62] Germano, M., Piomelli, U., Moin, P., and Cabot, W., "A Dynamic Subgrid-Scale Eddy Viscosity Model," *Physics of Fluids A*, Vol. 3, No. 7, 1991, pp. 1760–1765. doi:10.1063/1.857955
[63] Moin, P., Squires, W., Cabot, W., and Lee, S., "A Dynamic Subgrid-Scale Model for Compressible Turbulence and Scalar Transport," *Physics of Fluids A*, Vol. 3, No. 11, 1991, pp. 2746–2757. doi:10.1063/1.858164
[64] Lily, D. K., "A Proposed Modication of the Germano Sugrid-Scale Closure Method," *Physics of Fluids A*, Vol. 4, No. 3, 1992, pp. 633–635. doi:10.1063/1.858280
[65] Yakhot, A., Orszag, S. A., and Israeli, M., "Renormalization Group Formulation of Large-Eddy Simulation," *Journal of Scientific Computing*, Vol. 1, 1986, pp. 3–51. doi:10.1007/BF01061452
[66] Kim, W.-W., and Menon, S., "LES of Turbulent Fuel/Air Mixing in a Swirling Combustor," AIAA Paper 980-0200, Jan. 1999.
[67] Suresh, M., and Stone, C., "Simulation of a Fuel-Air Mixing Combustion in a Trapped-Vortex Combustor," AIAA Paper 2000-0478, Jan. 2000.
[68] O'Brien, E. E., "The Probability Density Function (PDF) Approach to Reacting Turbulent Flows," *Turbulent Reacting Flows*, edited by P. A. Libby, and F. A. Williams, Chap. 5, Springer–Verlag, Heidelberg, 1980, pp. 185–218.
[69] Pope, S. B., "PDF Methods for Turbulent Reacting Flows," *Progress in Energy and Combustion Science*, Vol. 11, No. 2, 1985, pp. 119–192. doi:10.1016/0360-1285(85)90002-4
[70] Lundgren, T. S., "Model Equation for Nonhomogeneous Turbulence," *Physics of Fluids*, Vol. 12, No. 3, 1969, pp. 485–497. doi:10.1063/1.1692511
[71] Pope, S. B., "The Probability Approach to Modeling of Turbulent Reacting Flows," *Combustion and Flame*, Vol. 27, Aug.–Dec. 1976, pp. 299–312. doi:10.1016/0010-2180(76)90035-3
[72] Germano, M., "Turbulence: The Filtering Approach," *Journal of Fluid Mechanics*, Vol. 238, May 1992, pp. 325–336. doi:10.1017/S0022112092001733
[73] Salvetti, M. V., and Banerjee, S., "A Priori Tests of a New Dynamic Subgrid-Scale Model for Finite-Difference Large-Eddy Simulations," *Physics of Fluids*, Vol. 7, No. 11, 1995, pp. 2831–2847. doi:10.1063/1.868779
[74] Dopazo, C., and O'Brien, E. E., "Statistical Treatment of Non-Isothermal Chemical Reactions in Turbulence," *Combustion Science and Technology*, Vol. 13, July 1976, pp. 99–122. doi:10.1080/00102207608946731
[75] Borghi, R., "Turbulent Combustion Modeling," *Progress in Energy and Combustion Science*, Vol. 14, No. 4, 1988, pp. 245–292. doi:10.1016/0360-1285(88)90015-9
[76] Yu, H., Luo, L.-S., and Girimaji, S. S., "Scalar Mixing and Chemical Reaction Simulations Using Lattice Boltzmann Method," *International Journal of Computational Engineering Science*, Vol. 3, No. 1, 2002, pp. 73–78. doi:10.1142/S1465876302000551
[77] Lele, S. K., "Compact Finite Difference Schemes with Spectral-Like Resolution," *Journal of Computational Physics*, Vol. 103, No. 1, Nov. 1992, pp. 16–42. doi:10.1016/0021-9991(92)90324-R
[78] Visbal, M. R., and Gaitonde, D. V., "Very High-Order Spatially Implicit Schemes for Computational Acoustics on Curvilinear Meshes," *Journal of Computational Acoustics*, Vol. 9, No. 4, 2001, pp. 1259–1286.
[79] Shu, C. W., and Osher, S., "Efficient Implementation of Essentially Non-Oscillatory Shock-Capturing Schemes," *Journal of Computational Physics*, Vol. 77, No. 2, Aug. 1988, pp. 439–471. doi:10.1016/0021-9991(88)90177-5
[80] Gottlieb, S., Shu, C. W., and Tadmor, E., "Strong Stability-Preserving High-Order Time Discretization Methods," *SIAM Review*, Vol. 43, No. 1, 2001, pp. 89–112. doi:10.1137/S003614450036757X
[81] Gaitonde, D. V., and Visbal, M. R., "A Further Development of a Navier–Stokes Solution Procedure Based on High-Order Formulas Simulation," AIAA Paper 99-0557, Jan. 1999.
[82] Jameson, A., and Baker, T., "Solutions of the Euler Equations for Complex Congurations," AIAA Paper 83-1929, 1983.
[83] Poinsot, T., and Lele, S., "Boundary Conditions for Direct Numerical Simulations of Compressible Viscous Flows," *Journal of Computational Physics*, Vol. 101, No. 1, July 1992, pp. 104–129. doi:10.1016/0021-9991(92)90046-2
[84] Pope, S. B., "Particle Method for Turbulent Flows: Integration of Stochastic Model Equations," *Journal of Computational Physics*, Vol. 117, No. 2, March 1995, pp. 332–349. doi:10.1006/jcph.1995.1070
[85] Risken, H., *The Fokker-Planck Equation, Methods of Solution and Applications*, Springer–Verlag, New York, 1989.
[86] Gardiner, C. W., *Handbook of Stochastic Methods*, Springer–Verlag, New York, 1990.
[87] Karlin, S., and Taylor, H. M., *A Second Course in Stochastic Processes*, Academic Press, New York, 1981.
[88] Pope, S. B., "Lagrangian PDF Methods for Turbulent Flows," *Annual Review of Fluid Mechanics*, Vol. 26, Jan. 1994, pp. 23–63. doi:10.1146/annurev.fl.26.010194.000323
[89] Grigoriu, M., *Applied Non-Gaussian Processes*, Prentice–Hall, Englewood Cliffs, NJ, 1995.
[90] Kloeden, P. E., Platen, E., and Schurz, H., *Numerical Solution of Stochastic Differential Equations Through Computer Experiments*, Springer–Verlag, New York, corrected second printing edition, 1997.
[91] Haworth, D. C., and Pope, S. B., "A Second-Order Monte Carlo Method for the Solution of the Ito Stochastic Differential Equation," *Stochastic Analysis and Applications*, Vol. 4, No. 2, 1986, pp. 151–186. doi:10.1080/07362998608809086
[92] Haworth, D. C., and Pope, S. B., "Monte Carlo Solutions of a Joint PDF Equation for Turbulent Flows in General Orthogonal Coordinates," *Journal of Computational Physics*, Vol. 72, No. 2, 1987, pp. 311–346. doi:10.1016/0021-9991(87)90086-6
[93] Xu, J., and Pope, S. B., "Assessment of Numerical Accuracy of PDF/Monte Carlo Methods for Turbulent Reacting Flows," *Journal of Computational Physics*, Vol. 152, No. 1, June 1999, pp. 192–230. doi:10.1006/jcph.1999.6241
[94] Kloeden, P. E., and Platen, E., *Numerical Solution of Stochastic Differential Equations*, Vol. 23, Applications of Mathematics, Stochastic Modelling and Applied Probability, Springer–Verlag, New York, 1995.
[95] Billingsly, P., *Probability and Measure*, Wiley, New York, 1979.
[96] Gillespie, D. T., *Markov Processes, An Introduction for Physical Scientists*, Academic Press, New York, 1992.
[97] Ito, K., "On Stochastic Differential Equations," *Memoirs of American Mathematical Society*, Vol. 4, American Mathematical Society, Providence, RI, 1951, pp. 1–151.
[98] Gikhman, I. I., and Skorokhod, A. V., *Stochastic Differential Equations*, Springer–Verlag, New York, 1995.
[99] Muradoglu, M., Jenny, P., Pope, S. B., and Caughey, D. A., "A Consistent Hybrid-Volume/Particle Method for the PDF Equations of Turbulent Reactive Flows," *Journal of Computational Physics*, Vol. 154, No. 2, Sept. 1999, pp. 342–371. doi:10.1006/jcph.1999.6316
[100] Muradoglu, M., Pope, S. B., and Caughey, D. A., "The Hybrid Method for the PDF Equations of Turbulent Reactive Flows: Consistency Conditions and Correction Algorithms," *Journal of Computational Physics*, Vol. 172, No. 2, Sept. 2001, pp. 841–878. doi:10.1006/jcph.2001.6861
[101] Sheikhi, M. R. H., Drozda, T. G., Givi, P., and Pope, S. B., "Velocity-Scalar Filtered Density Function for Large Eddy Simulation of Turbulent Flows," *Physics of Fluids*, Vol. 15, No. 8, July 2003, pp. 2321–2337. doi:10.1063/1.1584678
[102] Gillandt, I., Fritsching, U., and Bauckhage, K., "Measurement of Phase Interaction in Dispersed Gas/Particle Two-Phase Flow," *International Journal of Multiphase Flow*, Vol. 27, No. 8, Aug. 2001, pp. 1313–1332. doi:10.1016/S0301-9322(01)00007-6
[103] Shih, T.-P., Bailey, R., Nguyen, H., and Roelke, R. J., "Algebraic Grid

Generation for Complex Geometries," *International Journal for Numerical Methods in Fluids*, Vol. 13, No. 1, 1991, pp. 1–31. doi:10.1002/fld.1650130102

[104] Steinthorsson, E., Shih, T.-P., and Roelke, R. J., "Enhancing Control of Grid Distribution in Algebraic Grid Generation," *International Journal for Numerical Methods in Fluids*, Vol. 15, No. 3, 1992, pp. 297–311. doi:10.1002/fld.1650150304

[105] Rudy, D. H., and Strikwerda, J. C., "Boundary Conditions For Subsonic Compressible Navier–Stokes Calculations," *Computers and Fluids*, Vol. 9, No. 3, Sept. 1981, pp. 327–338. doi:10.1016/0045-7930(81)90005-0

[106] Pope, S. B., *Turbulent Flows*, Cambridge Univ. Press, Cambridge, U.K., 2000.

H. Chelliah
Associate Editor